

Boussinesq modelling of transient rip currents

D. Johnson^{*}, C. Pattiaratchi

Centre for Water Research, University of Western Australia, 35 Stirling Highway, Crawley, WA 6011, Australia

Received 10 January 2005; received in revised form 24 August 2005; accepted 24 November 2005
Available online 25 January 2006

Abstract

The flow on a plane beach with a random, directionally spread wave field was simulated with a Boussinesq model. The random wave spectra were directionally symmetric with their central direction perpendicular to the beach, so no constant longshore current was generated. Variable wave-averaged currents were generated because of the spatially variable wave field, and sometimes formed offshore directed rip currents that appear in variable longshore locations. The rip currents are associated with a vortex pair which is generated within the surfzone and subsequently propagates offshore. Analysis of the vorticity balance show that the main vorticity input occurs within the inner surfzone. Three different beach slopes and four different wave spectra are simulated. The frequency, duration, and intensity of the transient rips depend on both the beach slope and the incident wave spectra. The results have important engineering implications for the transport of material in the nearshore zone, in particular on longshore uniform beaches.

© 2005 Elsevier B.V. All rights reserved.

Keywords: Modelling; Boussinesq model; Surfzone; Rip currents

1. Introduction

Transient rips are narrow offshore flows generated in the surfzone. Unlike rip currents which are associated with a topographic rip channel, transient rips are spatially and temporally variable, and are temporary features which develop, have a specific lifetime and then decay. Importantly, they are not restricted to well-defined topographic variation and can occur on long shore uniform beaches.

Rip currents are generated by longshore inhomogeneities in the momentum flux gradient of the incident wave field, which can be caused by differential wave transformation over variable topography, as occurs over a rip channel in a longshore bar. However, the nearshore wave field can possess longshore variations in the onshore momentum flux on a plane, featureless beach, caused by

- (1) Interaction of the incident wave field and the wave-averaged mean current (Dalrymple and Lozano, 1978; LeBlond and Tang, 1974).

- (2) Interaction of the incident wave field with lower frequency waves such as edge waves (Bowen, 1969; Sasaki and Horikawa, 1978; Symonds and Ranasinghe, 2001).
- (3) The inherent spatial variability of the incident wave field (Dalrymple, 1975; Tang and Dalrymple, 1989; Peregrine, 1998).

Transient rips of the second (Bowen and Inman, 1969) and third (Dalrymple, 1975; Fowler and Dalrymple, 1991; Hammack et al., 1991) types have been generated in the laboratory. There have been few measurements of transient rips in the field; Tang and Dalrymple (1989) made measurements of nearshore circulation, including (transient) rips, which were spatially and temporally variable and concluded that they were largely driven by the variability of the incident wave field. Johnson and Pattiaratchi (2004) (hereafter JP04) recently made Lagrangian measurements of transient rips where the swell was perpendicularly incident on a beach without an offshore bar or significant longshore variation. The trajectories showed narrow (length scales 20–30 m) offshore directed flows with typical flow speeds $0.2\text{--}0.5\text{ ms}^{-1}$ occurring at variable locations. The Lagrangian velocities showed that forcing occurs mainly at the start of the

^{*} Corresponding author. Present address: MetOcean Solutions Limited, Suite 3, 17 Nobs Line, New Plymouth, New Zealand.

E-mail address: d.johnson@metocean.co.nz (D. Johnson).

rip neck and that the neck subsequently spreads into a head region outside the surfzone. Eulerian measurements from the same experiment strongly supported the assertion that the rips did not persist at one location.

The usual definition of the nearshore current is the net flow after averaging over the incident short wave motion. Vertical averaging then defines a wave and depth-averaged current vector, $\bar{\mathbf{U}}$ which is governed by:

$$\frac{\partial \bar{\eta}}{\partial t} + \nabla \cdot [(\bar{\eta} + h)\bar{\mathbf{U}}] = 0 \quad (1)$$

$$\frac{\partial \bar{\mathbf{U}}}{\partial t} + (\bar{\mathbf{U}} \cdot \nabla)\bar{\mathbf{U}} = -g\nabla \bar{\eta} + \mathbf{S} + \mathbf{L} + \mathbf{B} \quad (2)$$

where h is the still water depth, $\bar{\eta}$ is the wave-averaged surface elevation, \mathbf{S} is short wave forcing, \mathbf{L} is a term to describe lateral mixing, and \mathbf{B} is bottom friction. Eqs. (1) and (2) are a set of forced shallow water equations, and with various simplifications are the theoretical basis for most descriptions of nearshore flow at frequencies below that of the incident waves.

To date most wave-averaged models solving Eqs. (1) and (2) have used wave drivers including shoaling, refraction, diffraction and wave-current interaction, but usually assume a homogeneous incoming wave field. As a result, the spatial variation of incident wave forcing is due to either variable mean water depth or interaction with the current. If there is feedback between the mean current/elevation field and the determination of the wave forcing, the first two transient rip generation mechanisms on a plane beach can be represented. Progress on more realistic wave-drivers (e.g. Kennedy and Kirby, 2003; van Dongeren et al., 2003) allows the spatial and temporal variation in the incident wave field to be modelled as well, thus potentially including the third rip generation mechanism even on longshore uniform bathymetry. Recent work by Reniers et al. (2004) shows the development of circulation cells on a longshore uniform beach when a spatially variable wave field forcing is used.

An alternative modelling approach used in this work is to actually resolve the incident wave field. Boussinesq-type equations (for a recent review, see Madsen and Schaffer, 1998) allow accurate simulation of surface waves from intermediate depth to shallow water. Simulation of a random wave field is possible, thereby implicitly including a spatially and temporally variable forcing of the wave-averaged currents. Furthermore, it also includes generation of vertical vorticity due to discontinuities in individual wave crests, something Peregrine (1998) has proposed as an important source of surfzone vorticity. Despite their potential for simulating complex hydrodynamics associated with random wave fields, they have received relatively little use for nearshore process research on open beaches; exceptions are Chen et al. (2003) and Kirby and Chen (2003) who simulated longshore currents at field scale.

This article reports the results of a modelling investigation of transient rip currents using a Boussinesq model. The model is

first described, and details of its implementation for simulating four different idealised random wave fields on plane beaches, with slopes of 0.05, 0.03 and 0.015, are presented. A qualitative validation of the model is provided by showing that transient rips, consistent with field measurements, are generated. The results of the modelling experiments are presented with three primary aims:

- To demonstrate that a Boussinesq simulation of a fully random wave field with mean direction perpendicular to a plane beach generates spatially variable wave-averaged currents, including well-defined transient rip currents.
- To investigate the forcing mechanism and vorticity balance for transient rip currents.
- To quantify the effect of varying wave fields and beach slopes on transient rip activity.

2. Model implementation

The numerical modelling was carried out using a modified version of *Funwave*, an open source distribution of a model developed at *The Center for Applied Coastal Research, University of Delaware*. *Funwave* is based on the fully non-linear Boussinesq equations of Wei et al. (1995), with an additional term to include vertical vorticity conservation at second order in the dispersive parameter as described by Chen et al. (2003). For completeness and for the context of the subgrid parameters detailed later, an outline of the model follows, including the governing equations, treatment of wave breaking, subgrid mixing and boundary conditions. Detailed description of the model subgrid schemes can be found in Kirby et al. (1998a), Kennedy et al. (2000) and Chen et al. (2000).

The equation for the conservation of mass is:

$$\beta \eta_t + \nabla \cdot \mathbf{M} + F_s = 0 \quad (3)$$

$$\mathbf{M} = \mathcal{A} \left[\mathbf{u} + \left(\frac{z_r^2}{2} - \frac{1}{6}(h^2 - h\eta + \eta^2) \right) \nabla(\nabla \cdot \mathbf{u}) + \left(z_r + \frac{1}{2}(h - \eta) \right) \nabla(\nabla \cdot (h\mathbf{u})) \right] \quad (4)$$

where $\mathbf{u}=(u,v)$ is the horizontal velocity vector at a reference depth of $z_r=-0.531h$. Subscript t denotes time differentiation. The still water depth is h , and η is the instantaneous surface elevation. The parameters β and \mathcal{A} account for the presence of slots, which simulate the presence of the beach face, in the vicinity of the shoreline. The term F_s is a source function which operates along a strip in the seaward region of the domain; this effectively adds and subtracts mass from this strip, thereby generating waves.

The momentum equation is:

$$\mathbf{u}_t + (\mathbf{u} \cdot \nabla)\mathbf{u} + g\nabla \eta + V_1 + V_2 + V_3 - F_{br} - F_m + F_b = 0 \quad (5)$$

The terms F_{br} , F_m and F_b account for wave breaking, lateral momentum mixing and bottom friction. V_1 and V_2 are dispersive terms:

$$V_1 = \frac{z_r^2}{2} \nabla(\nabla \cdot \mathbf{u}) + z_r \nabla(\nabla \cdot (h\mathbf{u})) - \nabla \left[\frac{\eta^2}{2} \nabla \cdot \mathbf{u}_t + \eta \nabla \cdot (h\mathbf{u}_t) \right] \quad (7)$$

$$V_2 = \nabla \left\{ (z_r - \eta)(\mathbf{u} \cdot \nabla)[\nabla \cdot (h\mathbf{u})] + \frac{1}{2}(z_r^2 - \eta^2)(\mathbf{u} \cdot \nabla)(\nabla \cdot \mathbf{u}) \right\} + \frac{1}{2} \nabla \{ [\nabla \cdot (h\mathbf{u}) + \eta \nabla \cdot \mathbf{u}]^2 \} \quad (8)$$

and V_3 is a second order correction to the vorticity (Chen et al., 2003):

$$V_3 = \mathbf{u} \times \left[\nabla \times \left\{ (z_r - z) \nabla[\nabla \cdot (h\mathbf{u})] + \left(\frac{z_r^2}{2} - \frac{z^2}{2} \right) \nabla(\nabla \cdot \mathbf{u}) \right\} \right] \quad (9)$$

where \times and $\nabla \times$ are the two-dimensional cross product and curl. Eqs. (3) and (5) are solved with a quasi fourth-order finite difference scheme (Wei et al., 1995).

Wave breaking is modelled with an eddy viscosity formulation which redistributes momentum and dissipates energy locally at the front face of the wave. The breaking term is given by:

$$F_{br} = \frac{1}{(h + \eta)} \{ \nabla \cdot \nabla [v_b(h + \eta)\mathbf{u}] + \nabla(\nabla \cdot [v_b(h + \eta)\mathbf{u}]) \} \quad (10)$$

$$v_b = BL^2 |(h + \eta) \nabla \cdot \mathbf{M}| \quad (11)$$

where L is a mixing length coefficient set at 1.2, and B varies between 0 and 1 and represents the intensity of breaking from initiation to cessation. Breaking begins when $\eta_t \geq 0.35\sqrt{gh}$ and stops when $\eta_t < 0.15\sqrt{gh}$.

Sub-grid turbulent mixing is included using a Smagorinsky (1963) model which calculates an eddy viscosity based on the wave-averaged currents. The term F_m in the momentum equation is identical to Eq. (10) but with the viscosity, v_b replaced by:

$$v_t = c_m \Delta x \Delta y \left[\left(\frac{\partial U}{\partial x} \right)^2 + \left(\frac{\partial V}{\partial y} \right)^2 + \frac{1}{2} \left(\frac{\partial U}{\partial y} + \frac{\partial V}{\partial x} \right)^2 \right]^{\frac{1}{2}} \quad (12)$$

where U and V are mean velocity components averaged in blocks of two peak wave periods.

Bottom friction is approximated with a quadratic law:

$$F_b = \frac{f_b}{h + \eta} \mathbf{u} |\mathbf{u}|. \quad (13)$$

The seaward boundary and landward boundary have a sponge layer region which absorbs any outgoing waves. The run-up at the shoreline is modelled using a slot technique, in

which the beach is made semi-permeable and the solution domain includes the region where the beach is above the still water level. The incident wave field is input in the seaward region of the domain using a source function method (Wei et al., 1999) in which mass is effectively added and removed.

Random waves were generated in similar manner to that used for laboratory generation in wave tanks (for a review see Hughes, 1993), by assuming the wave field to be the summation of multiple components. To match the periodic boundary conditions, the directional bins at each frequency were then determined by the requirement that the longshore wave-number components are integer multiples of the longshore length. The end result is a matrix of spectral densities with associated frequencies and directions.

At the source line, the amplitude for the source function input was the surface elevation of a random wave field, generated by summing multiple wave components:

$$\eta^S(y, t) = \sum_{i=1}^{i=n_\omega} \sum_{j=1}^{j=n_\theta} a_{ij}^S \cos[k_i \sin \theta_j - \omega_i t + \phi_{ij} + \phi_{ij}^* t] \quad (14)$$

where f_i is the frequency, θ_j the direction relative to the x -axis, a_{ij}^S the Fourier amplitude and ϕ_{ij} a random phase component for the $[i, j]$ th component. The term ϕ_{ij} is a random phase, as is commonly used in random wave synthesis to prevent spurious phase coupling. Without the last term in the square bracket, the method is that described by Wei et al. (1999), and has been used by Chen et al. (2003) and Shi et al. (2003) for generating a random wave field in a Boussinesq model. The $\phi_{ij}^* t$ term is an additional random time dependent phase change which prevents the generation of a longshore stationary wave field. This reason for this addition term, and the discretization for the periodic domain are detailed below in Section 2.1. For each simulation using the same spectrum, the source input was identical, as the random seed was kept the same.

There are two limitations in how well Eq. (14) recreates the nearshore incident wave field for a given spectrum. Firstly, no bound long waves are included in the source function, which in reality would already be present and propagating with the wave groups into the model domain. Second, the random phase approximation results in a linear wave field at the boundary, whereas real waves would be somewhat nonlinear, and contain bound harmonics; however, visual observation of the surface elevation is that the incoming waves very quickly relax to an assymmetric form. As the numerical experiments in this work aim to investigate hydrodynamics forced by random wave fields incident on a beach in a general and idealised way, we do not believe the pertinent results are compromised by the lack of bound long waves or nonlinearity at the input boundary.

The open source code was modified to include the boundary conditions discussed above, input of the random wave field, and the vorticity correction (Chen et al., 2003) of the original momentum equation of Wei et al. (1995). The original Fortran code was also parallelised to run on a high performance computer.

Quite extensive testing and validation of *Funwave* has been reported in Kennedy et al. (2000) and Chen et al. (2001). The

simulations of laboratory (topographic) rip currents by Chen et al. (1999), and longshore currents at field scale (Chen et al., 2003; Kirby and Chen, 2003) showed good agreement with measured data.

2.1. Discretization of wave spectra

In order to satisfy the periodic boundary conditions, for each component in the wave field, with wave number k_i and direction θ_j (anticlockwise from an onshore directed x -axis), there must be an integer number of wavelengths in the cross-shore direction:

$$k_i \sin \theta_j = \frac{2\pi p}{L} = pk_D \quad (15)$$

where p is an integer and k_D is the wave number of the longshore domain length. A dispersion relation is assumed to be valid at the source line so that: $\omega_i = gk_i \tanh k_i h$. In practice, the directional wave spectrum, $\Phi(\omega_i, \theta_j)$, is first discretised into 100 frequency bins of equal energy, then the dispersion relation is inverted numerically to give a set of k_i . Then for each k_i , θ_j is determined by inverting Eq. (15) so that:

$$\theta_j = \arcsin\left(\frac{pk_D}{k_i}\right); p = j. \quad (16)$$

The amplitudes of the individual components are given by:

$$a_{ij}^S = \sqrt{2\Phi(\omega_i, \theta_j)\Delta\omega_i\Delta\theta_j} \quad (17)$$

where $\Delta\omega_i$ and $\Delta\theta_j$ are the bin dimensions for each component. Chen et al. (2003) successfully generated an obliquely incident random wave field with Eq. (14), discretised under the constraint of Eq. (15). However, in this work, the requirement of a symmetric wave field with mean direction perpendicular to the beach was found to lead to problems ensuring random forcing in terms of its longshore distribution. For a directionally symmetric spectrum with central direction perpendicular to the source line as is the case with spectrums used for the simulations, each spectral bin $[i, j]$ in Eq. (14) exists as one member of a pair of opposite directions. Denoting directional index pairs by $[i, j^+]$ and $[i, j^-]$ so that $\theta_{j^+} = -\theta_{j^-}$, Eq. (14) can be rewritten as:

$$\eta^S(y, t) = \sum_{i=1}^{i=n_\omega} \sum_{j=1}^{j=n_\theta^+} a_{ij^+}^S \cos[k_i \sin \theta_{j^+} - \omega_i t + \phi_{ij^+}] + a_{ij^-}^S \cos[k_i \sin \theta_{j^-} - \omega_i t + \phi_{ij^-}] \quad (18)$$

which, as $\sin \theta_{j^+} = -\sin \theta_{j^-}$ and $a_{ij^+}^S = a_{ij^-}^S$, and by substituting Eq. (15) is equivalent to:

$$\eta^S(y, t) = \sum_{i=1}^{i=n_\omega} \sum_{j=1}^{j=n_\theta^+} 2a_{ij^+}^S \cos[\omega_i t + \phi_{ij^+}] \cos[jk_D y + \psi_{ij^+}] \quad (19)$$

where $\phi_{ij^+} = (\phi_{ij^+} + \phi_{ij^-})/2$ and $\psi_{ij^+} = (\phi_{ij^+} - \phi_{ij^-})/2$. Eq. (19) can be seen to represent a sum of longshore fixed standing waves, which must have wave numbers that are integer multiples of k_D . Furthermore, there is a large amount of energy in the first few

modes; as a result, there are fixed areas of high and low waves. When investigating forcing due to a random wave field on an otherwise homogeneous longshore domain, this is highly undesirable.

A number of methods were tested in order to overcome the problem of longshore stationarity in the incident wave field. These included:

- Non-symmetric discretisations of the spectrum into frequency/directional bins.
- A Nondeterministic Spectral Amplitude method (Hughes, 1993), which uses random Fourier coefficients (thereby varying the component amplitudes while still preserving the long-time averaged distribution of wave energy in the frequency/direction domain).
- A nondeterministic method that uses both random amplitudes and random (constant) perturbations to the frequencies in each bin, while again preserving the overall distribution of wave energy.

It was observed that the wave components in the above methods always combine to produce stationary longshore distributions of the time-averaged wave heights.¹ The eventual, admittedly somewhat ad hoc, method that worked well in practise was to include an additional dependent random term, $\chi_{ij} t$, in the phase function,

$$a^S(y, t) = \sum_{i=1}^{i=n_\omega} \sum_{j=1}^{j=n_\theta} a_{ij}^S \cos[k_i \sin(\theta_j) y - (\omega_i + \chi_{ij}) t + \phi_{ij}]. \quad (20)$$

This modifies Eq. (19) to:

$$a^S(y, t) = \sum_{i=1}^{i=n_\omega} \sum_{j=1}^{j=n_\theta^+} 2a_{ij^+}^S \cos[\omega_i t - \phi_{ij^+}^* + \psi_{ij^+}^*] \cos[k_i \sin \theta_{j^+} - \psi_{ij^+}^* t + \psi_{ij^+}^*] \quad (21)$$

where $\phi_{ij^+}^* = (\chi_{ij^+} + \chi_{ij^-})/2$ and $\psi_{ij^+}^* = (\chi_{ij^+} - \chi_{ij^-})/2$. Now the source line “standing waves” move alongshore with a celerity of $\psi_{ij^+}^*/k_i \sin \theta_{j^+}$. Note that this introduces a slight frequency shift in the fundamental wave as well, thus technically violating the dispersion relation. However, since the dispersion relation is not satisfied perfectly in the domain in any case due to nonlinearity, small values of χ_{ij} do not appear to cause problems in the source function. It was found that $\chi_{ij} = 0.1N\omega$, with N a uniformly distributed random number between 0 and 1, was a suitable value.

The longshore variance of the source line amplitudes were checked for the periodic case and a non-periodic source line without the restriction of Eq. (15):

$$v_1 = \frac{1}{n} \sum_{i=1}^n \text{Var}[a^S(y, t_i)] \quad (22)$$

$$v_2 = \text{Var}\left[\sqrt{\frac{1}{n} \sum_{i=1}^n a^S(y, t_i)^2}\right] \quad (23)$$

¹ An additional method we became aware of after the work was completed is to use only one direction for each frequency bin (van Dongeren et al., 2003).

where a^S is the source function amplitude for longshore position y at time-step t_i , and the variance is along the y (longshore) variable in each case. For the least directionally spread spectra used in the numerical experiments (which should experience the greatest effect of having to satisfy Eq. (15)), the time averaged longshore variances are $\nu_1 = 4.9 \times 10^{-6}$ for the periodic case, and $\nu_1 = 3.6 \times 10^{-6}$ for a non-periodic source line. For ν_2 , which is a measure of the longshore variability of wave energy averaged over the whole simulation, values are 1.9×10^{-5} and 1.4×10^{-5} . So while the need to map to integer longshore wave lengths has increased the longshore variability, it has not done so significantly. More importantly, the small values for ν_2 show that fixed longshore locations of high and low waves have not been generated.

3. Experiments

3.1. Model domain

The domain for all the numerical experiments was a plane beach of varying slope as shown in Fig. 1. The coordinate axes are oriented with x directed cross-shore towards the shoreline, and y longshore. Grid spacing in the crossshore and longshore directions is 2 and 3 m respectively. For each slope, the outer wave generation region was kept the same, 7 m deep and 160 m long. The source line was located at $x=60$ m. The domain is periodic in the longshore direction with a length of 1191 m while the cross-shore length extends to beyond the limit of wave uprush and depends on the slope.

The slot width used for the shoreline run-up was $\delta=0.04$ and the shape parameter $\lambda=10$ which is rather too large for accurate simulation of wave run-up (Kennedy et al., 2000). This was the smallest slot size that could be used while maintaining numerical stability for all the simulations, and for the sake of consistency between runs, the same value was used throughout. Tests of different slot widths indicated that the resulting error

affects only the swash zone; the setup further out is very similar so the error is unlikely to be important for the dynamics occurring away from the swash zone.

3.2. Wave spectra

The input wave spectra were directional spread TMA spectra (Bouws et al., 1985). A one-dimensional TMA spectrum was constructed for depth H with a peak frequency of f_p :

$$S(f, H) = \alpha g^2 (2\pi)^{-4} f^{-5} \Psi_1(f, H) \Psi_2(f/f_p) \Psi_3(f, f_p, \gamma, \mu_a, \mu_b)$$

$$\Psi_1(f, H) = \frac{[k(f, H)^{-3} \frac{\partial k(f, H)}{\partial f}]}{[k(f, \infty)^{-3} \frac{\partial k(f, \infty)}{\partial f}]}$$

$$\Psi_2(f/f_p) = \exp[-5/4(f/f_p)^{-4}]$$

$$\Psi_3(f, f_p, \gamma, \omega_a, \omega_b) = \exp[\ln(\gamma) \exp(-(f-f_p)^2/2\mu^2 f_p^2)]$$

$$\mu = \begin{cases} \mu_a & f_p \geq f \\ \mu_b & f_p < f \end{cases}$$

where k is the wave number for a particular depth and frequency. The dispersion relation, $\omega^2 = gk \tanh(kh)$ is assumed to be valid. Parameters used are: $\gamma=2$ $\alpha=0.014$ $\omega_a=0.07$ $\omega_b=0.09$.

The 1D frequency spectra were converted to directional spectra using a directional spreading function (Mitsuyasu, 1975):

$$\Phi(f, \theta) = S(f, H)G(\theta) \tag{24}$$

$$G(\theta) = \sum_i \omega \cos^{2D} \left(\frac{\theta - \theta_0}{2} \right) \tag{25}$$

where θ_0 is the peak direction and w is a weighting so that $\int G(\theta) d\theta = 1$. The value of D was varied to produce a spectrum with wide or narrow spreading.

For the simulations, four spectra with RMS wave height of 0.7 m were generated with the parameters in Table 1. The spectra

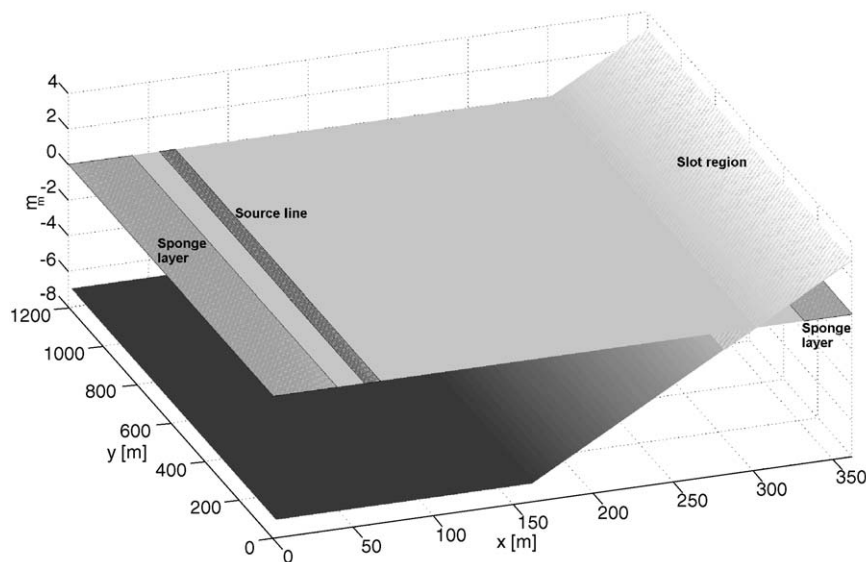


Fig. 1. Model domain.

Table 1
Parameters used for wave spectra

Spectra	T_p (s)	f_p (Hz)	f_{\min} (Hz)	f_{\max} (Hz)	θ_0	Σ_1
N10	10	0.1	0.02	0.3	0	100
N7	7	0.143	0.05	0.4	0	100
W7	7	0.143	0.05	0.4	0	10
W5	5	0.2	0.1	0.5	0	10
VN10	10	0.1	0.02	0.3	0	1000

The main direction, θ_1 , is measured relative to the x -axis. Frequencies are in 100 bins of equal energy bounded by f_{\min} and f_{\max} . The RMS wave height for all the spectra is 1.0 m.

are plotted in the left hand column in Fig. 2. Spectrum N10 is an ideal representation of swell with narrow spreading and N7 is shorter period waves with narrow spreading. Spectrum W5 corresponds to a locally generated, directionally spread sea,

while W7 is a longer period directionally spread sea. The aim was to compare the effects of period and spreading while using spectra which are still reasonable for natural conditions. The right hand column of Fig. 2 shows the spectra estimated using the Extended Maximum Likelihood Method (Isobe et al., 1984) from simulated data just shoreward of the source line generation region at $x=100$ m, $y=600$ m. Although the estimation method cannot retrieve the simulated directional spectrum perfectly, correspondence with the input spectra is good.

3.3. Simulation runs

A total of 17 runs were carried out. Runs 1–12 tested each beach slope with each spectra and are the main experimental simulations. Runs 13–16 were carried out to check the influence

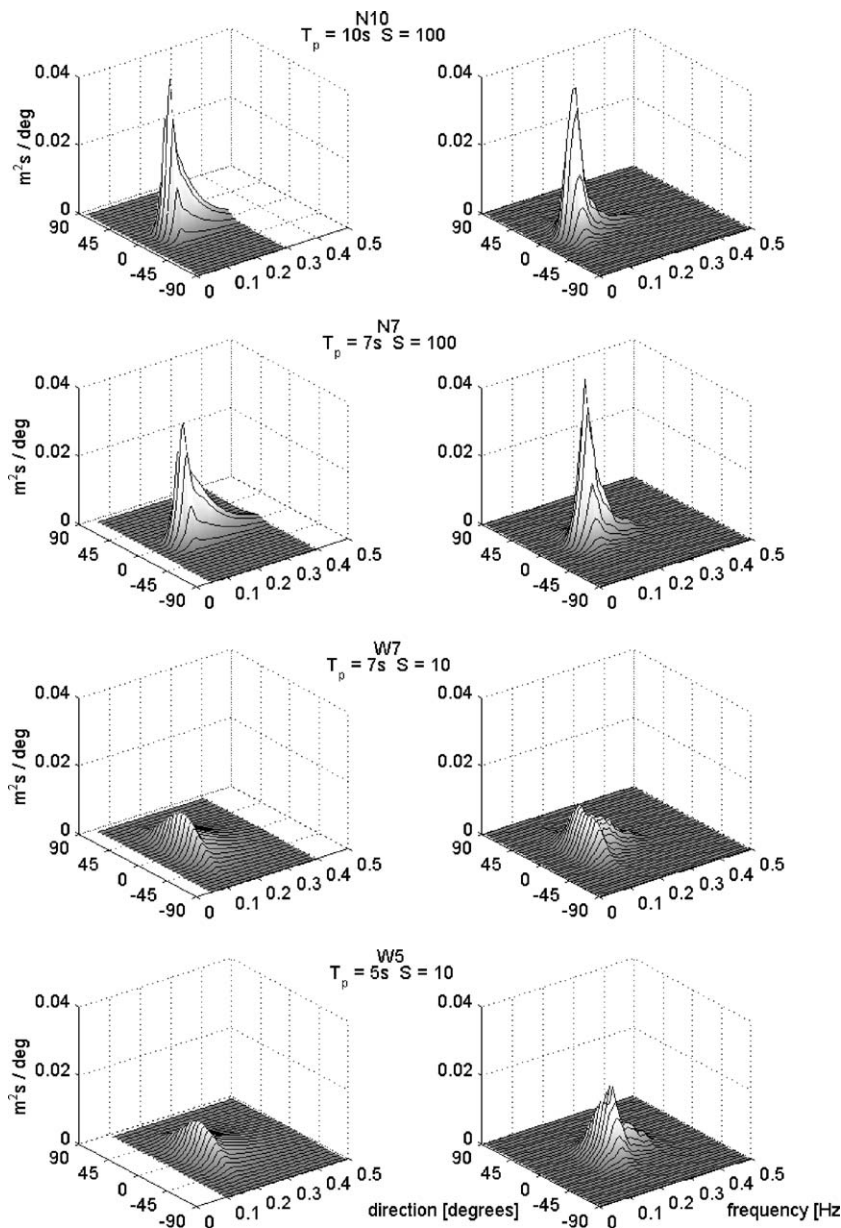


Fig. 2. Directional spectra used in the simulations. Directions are measured anticlockwise from the x -axis. The left column of subplots are the ETMA spectra input at the source line. The right column is the directional spectra estimated from the simulated surface elevation and velocities 50 m shoreward of the source line.

Table 2
Summary of simulation runs

Run	Abbrev.	Slope	Spec.	f_b	c_m
1	0.05N10	0.05	N10	0.001	0.2
2	0.05N7	0.05	N7	0.001	0.2
3	0.05W7	0.05	W7	0.001	0.2
4	0.05W5	0.05	W5	0.001	0.2
5	0.03N10	0.03	N10	0.001	0.2
6	0.03N7	0.03	N7	0.001	0.2
7	0.03W7	0.03	W7	0.001	0.2
8	0.03W5	0.03	W5	0.001	0.2
9	0.015N10	0.015	N10	0.001	0.2
10	0.015N7	0.015	N7	0.001	0.2
11	0.015W7	0.015	W7	0.001	0.2
12	0.015W5	0.015	W5	0.001	0.2
13	–	0.03	N10	0.01	0.2
14	–	0.03	N10	0.0001	0.2
15	–	0.03	N10	0.001	2.0
16	–	0.03	N10	0.001	0.02
17	–	0.03	VN10	0.001	0.2

of the turbulent mixing coefficient and bottom friction coefficient for the same conditions as run 5. Finally, run 17 was for a spectra with an unrealistically narrow spread on the 0.03 beach slope; this wave field has so little directional spreading that all waves are effectively perpendicular to the beach but still induces a small alongshore perturbation to the incident wave forcing. The model runs are summarised in Table 2.

The subgrid parameters were all identical except for the turbulent mixing coefficient and bottom friction coefficient. Closely following the values of Chen et al. (2003) for field scale simulation of longshore currents, values of $c_m = 0.2$ and $f_b = 0.001$ were used for the main set of simulations. The time-step was set to 0.1 s for all runs and each simulation ran for 50,000 time-steps or 5000 s, with the exception of runs 13–16 which were only run for 10,000 time-steps (1000 s). All times in the text or figures are relative to $t = 0$ s at the (cold) start of the simulations.

4. Model results

The model solution is a time series of instantaneous surface elevation and velocities at the reference height. The instanta-

neous mass flux, \mathbf{M} , was also retrieved. From the instantaneous mass flux and elevations, a wave-averaged mass flux, $\overline{\mathbf{M}}$ and surface elevation, $\overline{\eta}$ is defined, where the overline indicates averaging the instantaneous values over blocks of two peak wave periods, T_p .

A depth and wave-averaged velocity is then given by $\overline{\mathbf{U}} = \overline{\mathbf{M}} / (\overline{\eta} + d)$. To avoid infinite depth average current at the shoreline, $\overline{\mathbf{U}} = \mathbf{u}(\mathbf{r})$ for $\overline{\eta} + d < 0.2$, justified on physical grounds by the fact that any resolvable waves will be shallow water waves at this depth. The vorticity of the currents is defined as $\zeta = \nabla \times \overline{\mathbf{U}}$. Unless stated otherwise, the terms current and vorticity will refer to the depth and wave-averaged definitions. The averaging is effectively a filtering operation with lowpass cutoff of $f = 1 / 2T_p$. Note that the filtered current is not equivalent to the wave-averaged current in the classic wave-averaged sense, due to violation of the usual assumption that $\overline{\mathbf{U}}(\mathbf{u} - \overline{\mathbf{U}}) = 0$.

4.1. Instantaneous and wave-averaged flow

Fig. 3 shows a snapshot of the instantaneous surface elevation for run 5 (slope 0.03 and narrow spectrum with peak period 10 s). The waves can be seen to shoal and become increasingly asymmetric as they approach the shore, eventually decreasing in height as they break near the shoreline. The wave crests are not continuous, possessing two types of discontinuity: regions where two or more wave crests meet and areas at which a wave crest ends.

The instantaneous velocities are dominated by the wave orbital velocities. However, the vorticity of the instantaneous flow is very persistent, being advected and modulated due to vortex stretching by the passing waves, but varying over a much longer time scale. This is seen in a series of snapshots of instantaneous vorticity and velocity in Fig. 4; although there is significant local influence as the incident wave moves through, the net result is a relatively small change to the vorticity field. Also noticeable in the series of snapshots is the shedding of vorticity from the ends of breaking wave crests.

The currents show complex flow patterns in all of the runs except run 17. Fig. 5 shows mean flow vectors and vorticity

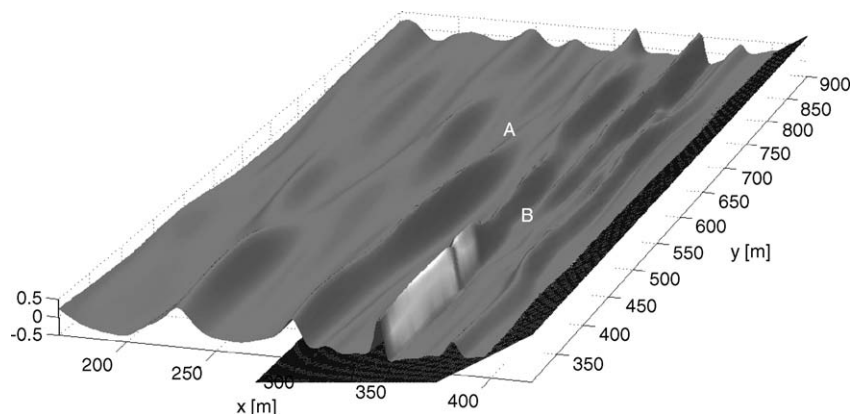


Fig. 3. Instantaneous surface elevation for run 5 at $t = 4160$ s for the centre of the longshore extent of the domain. The light coloured region at the front edge of one of the crest is a region of intense breaking. Two types of discontinuities in wave crests are indicated: A. End point of an individual wave crest. B. Merging of separate wave crests.

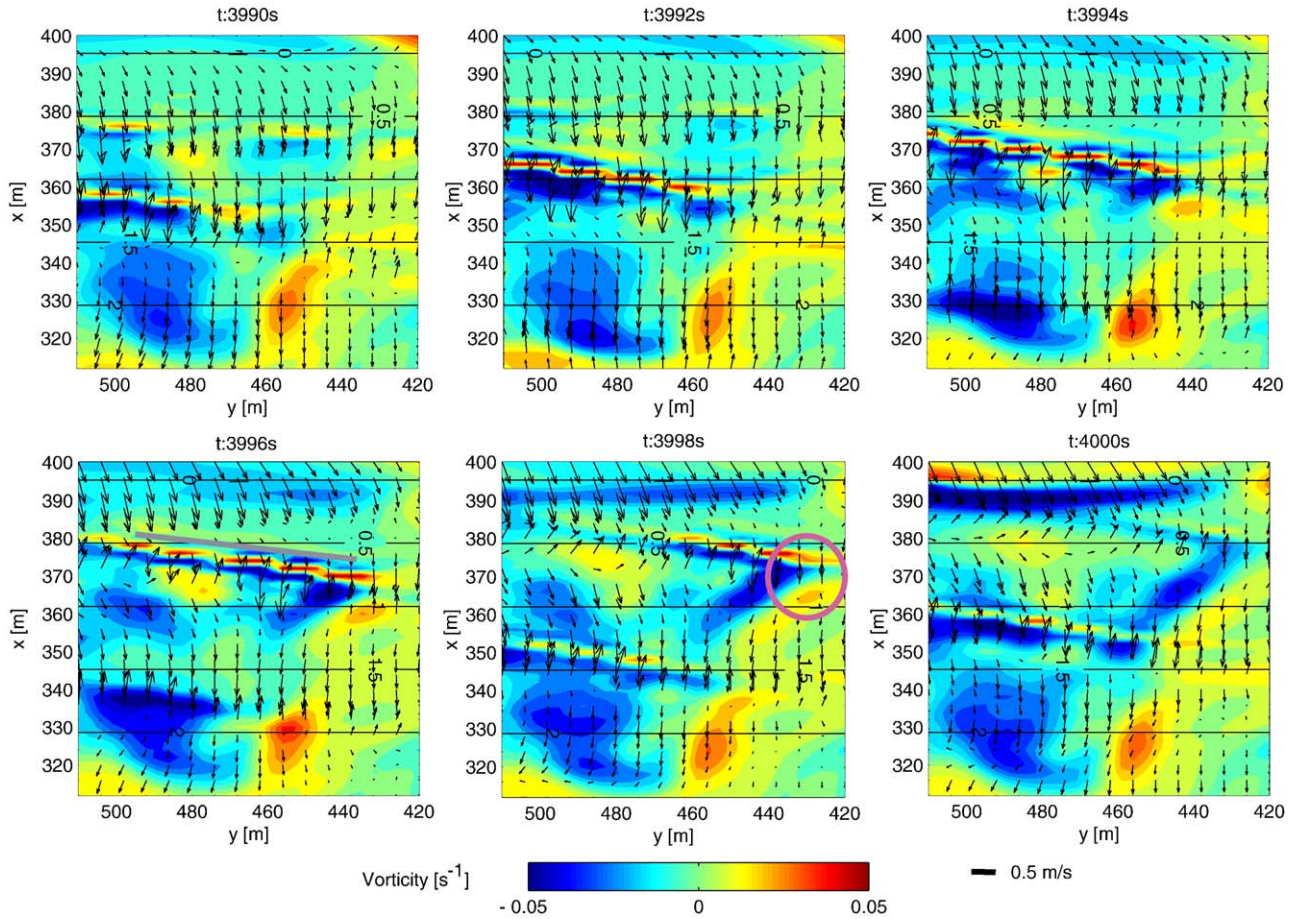


Fig. 4. Series of snapshots of an instantaneous velocity and vorticity. The lines of adjacent positive and negative vorticity are caused by breaking wave crests, as indicated by the line in frame $t=3996$ s. The circle in the frame for $t=3998$ s highlights shedding of negative vorticity from the end of the wave crest.

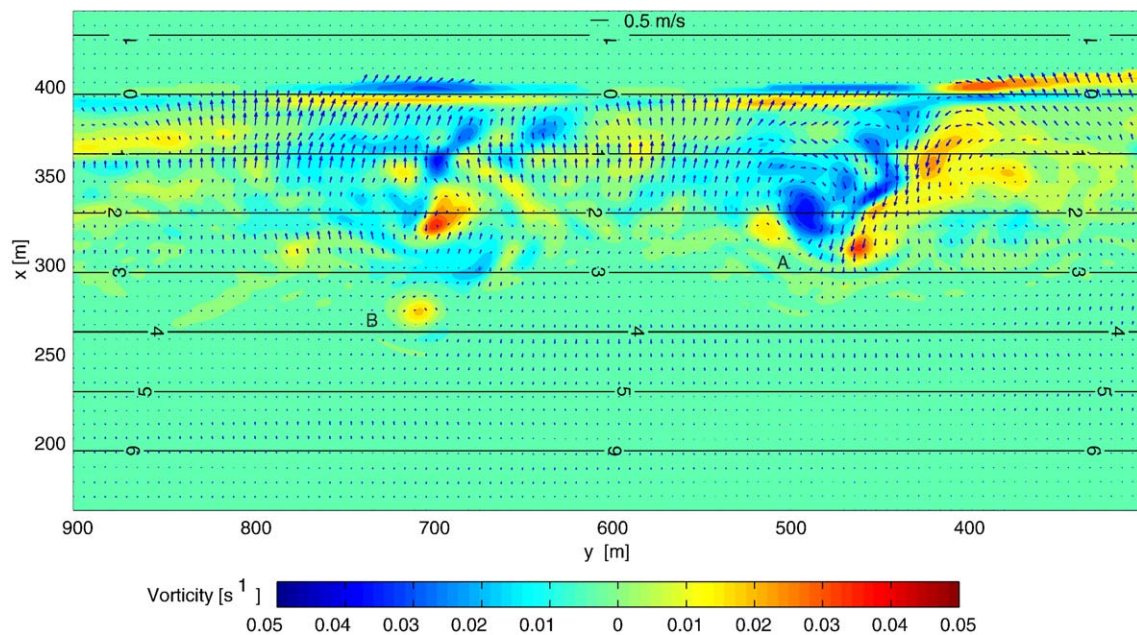


Fig. 5. Wave and depth-averaged current for run 5 at $t=4160$ s for the centre of the longshore extent of the domain. A rip current (A.) and discrete vortices (B.) can be seen, clearly associated with regions of strong vorticity.

(these are for the same time as the instantaneous surface in Fig. 3). The existence of discrete vortices (eddies) and more complex features, like transient rip currents, are seen in all of the wave and depth-averaged current fields. The transient rip currents appear as narrow regions of offshore flow which penetrate offshore and are associated with a vortex pair in the head. The offshore penetration of the rip currents is limited, reaching the 4 m contour in some of the beach slope/spectra conditions, but not beyond. The rip currents are oriented at varying angles to the shore but always have opposite regions of vorticity along the rip neck and a vortex pair in the head region.

Fig. 6 shows the trajectories of virtual particles released in the transient rip feature shown in Fig. 5. The trajectories were calculated by integrating the particle positions forward in time with the instantaneous model velocities. Small velocity fluctuations, consistent with the subgrid eddy viscosity, were also added to simulate subgrid turbulence. With a directionally narrow swell and a beach slope of 0.03, these conditions are very similar to those during the drifter deployments described in JP04; the measured trajectories of one of the sampled transient rip currents is shown in the lower plot of Fig. 6. There is strong qualitative similarity between the modelled and measured currents, with the modelled and measured trajectories showing the same features with very similar length scales.

The vorticity field of the wave-averaged currents has vortices and vorticity gradients at a range of scales and there are similarities with the rotational (in the sense of possessing vertical vorticity) flow seen in nonlinear simulations of longshore current instabilities (Allen et al., 1996; Ozkan-Haller and Kirby, 1999). The presence of low frequency waves can also be seen in the current fields as linear regions of similar flow velocities, but being irrotational, are not seen in the vorticity plots. While the existence of both rotational and long wave currents is ubiquitous, there is significant difference in the appearance of the current field for the different spectra and beach slopes. To illustrate this, the central sections from six different simulations (in order, runs 5, 6, 7, 8, 1, 9) are shown in Fig. 7. These compare the four spectra on the intermediate beach slope, 0.03, and the three beach slopes for the spectra, N10. Qualitative differences between the wave spectra are fewer, but better defined, vortical features for the narrow spread spectra, N10 and N7, compared to W7 and W5. However, the wide spread spectra appear to generate a more even spread of smaller vortices. There is a clear difference between beach slopes for the N10 spectra, as the milder slope, 0.015 has larger and more intense vortical structures than 0.03, whereas the steep slope, 0.05, has no discernable rotational features at the same vorticity shading scale.

As determined from the distribution of breaking and shoaling of mean wave heights, the average breakpoint position is between 2.0 and 1.5 m depth, further offshore for the longer period waves. The furthest offshore extent of wave breaking in each case is around the 2.5 m depth contour and based on this, the maximum surfzone widths are 50, 83, 167 m for the beach slope of 0.05, 0.03 and 0.015 respectively. Depth contours are used as a relative measure of cross-shore location for different beach slopes and spectra.

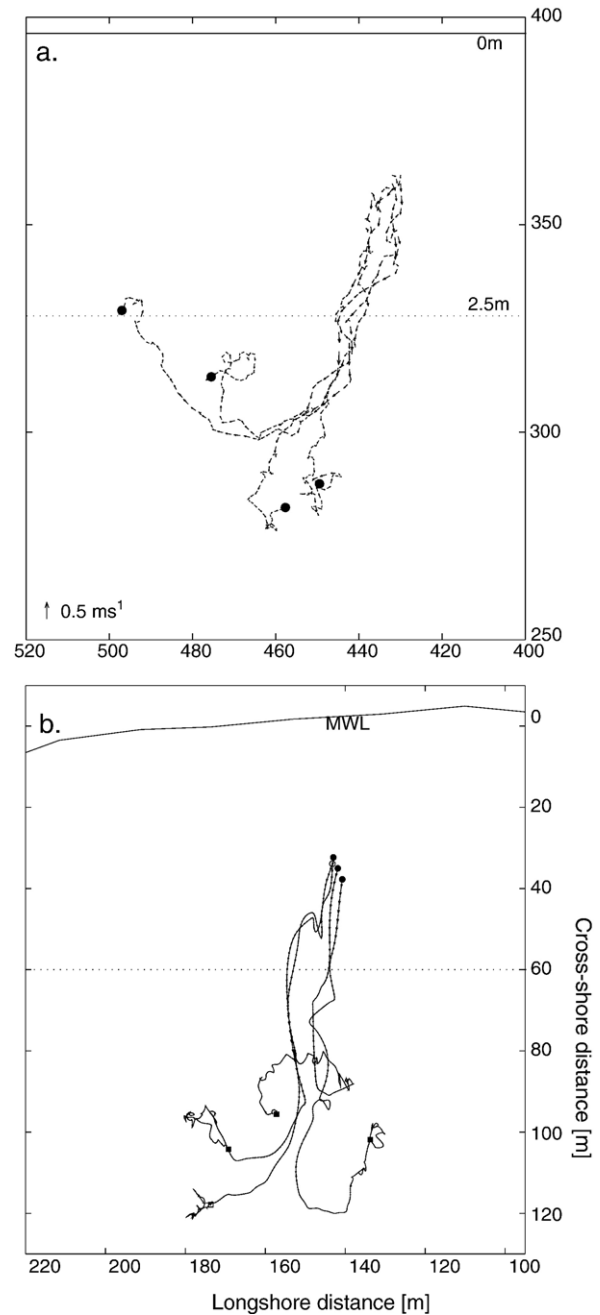


Fig. 6. a. Virtual drifter tracks from a deployment lasting 600 s of a cluster of drifters started at from $[x=360 \text{ m}, y=430 \text{ m}]$ at $t=4160 \text{ s}$ during run 5(0.03N10). b. Drifter trajectories from transient rip current measurements described in JP04. Wave conditions during the field measurements were swell dominated with a significant wave height of 1.02 m and the outer surfzone beach slope was 0.0325.

4.2. Longshore time series

Contour plots of velocity and vorticity as a function of longshore distance and time were produced. These type of (y, t) plots are useful for identifying rip events and discrete vortex features. The (y, t) velocity plots (Fig. 8) show a mixture of the cross-shore long wave velocity, which appears as bands, and rip currents and vortices, which appear as isolated regions of cross-shore flow. The vorticity plots are the best way to identify

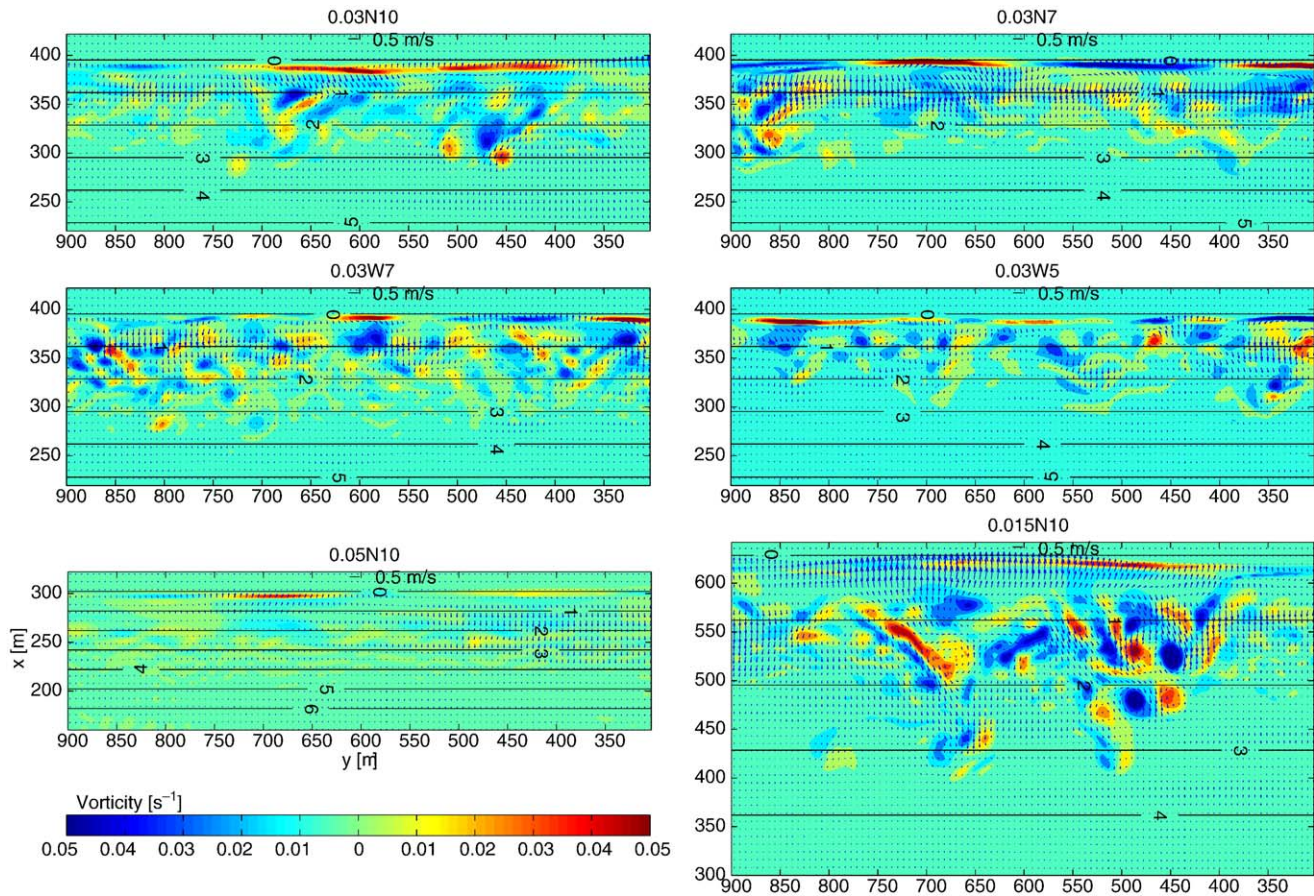


Fig. 7. Comparison of currents and vorticity for run 5 (0.03N10), 6 (0.03N7), 7 (0.03W7), 8 (0.03W5), 1 (0.05N10) and 9 (0.015N10) at $t=4700$ s.

features such as vortices and transient rips, as the long wave velocity signal, being irrotational, is effectively excluded. Rip currents and vortex pairs aligned alongshore appear as adjacent regions with opposite rotation whereas isolated vortices produce a signature with only positive or negative vorticity. The rip current in Fig. 5 is clearly seen as two strips of opposite signed vorticity. The gradient of a vortical feature in (y, t) space is its longshore propagation velocity. Most of the rip currents seen in Fig. 8 show little longshore movement during their lifetimes, but some do propagate longshore at up to 0.1 ms^{-1} .

The persistence of patches of vorticity is seen throughout the (y, t) plots, and associated narrow (in the longshore dimension) regions of offshore velocity can be discerned running through the cross-shore velocity plots. This is common to all the time series for the runs although there are differences between the spectra and beach slopes (Fig. 9); as would be expected from the snapshots in Fig. 7 of instantaneous vorticity, there are clear differences of frequency, spacing, intensity and duration of the vorticity patches. A quantitative comparison of the transient rip populations is carried out in Section 5.

Spectra of frequency and longshore wave number were calculated from the 2D Fourier transform from (y, t) to $k-\omega$ space. The spectra for the mean elevation and current along the 2.0 m isobath (Fig. 10) show the presence of infragravity waves, which exist at frequencies above the zeroth mode edge wave dispersion line, and another region of energy which lies

along the wave number axis at low frequencies. The second region cannot be due to infragravity waves as it is well outside the zeroth mode edge wave dispersion curve (Oltman-Shay et al., 1989) and the absence of energy in the surface elevation spectrum indicates a non-divergent motion. Shear waves would not be expected in the absence of longshore current and there is no evidence of a linear dispersion relation in $k-\omega$ space as is usually observed in shear waves (Oltman-Shay et al., 1989; Allen et al., 1996; Ozkan-Haller and Kirby, 1999). The conclusion is that the low frequency energy is associated with the rotational motion of the transient rip currents and vortices in the wave-averaged current. The same energy in this region of $k-\omega$ space was observed in the modelling results of Reniers et al. (2004), and was also associated with wave-averaged rotational flow caused by spatially variable wave forcing.

5. Comparison of transient rip occurrence

The snapshots of velocity and vorticity and the (y, t) plots show clear differences between beach slopes and wave spectra. As a measure of transient rip activity, the frequency, duration and velocity of individual rip currents were obtained for each beach slope/spectra regime.

In order to obtain the data on individual rip events, a rip must be identified in time and space, and to do this objectively

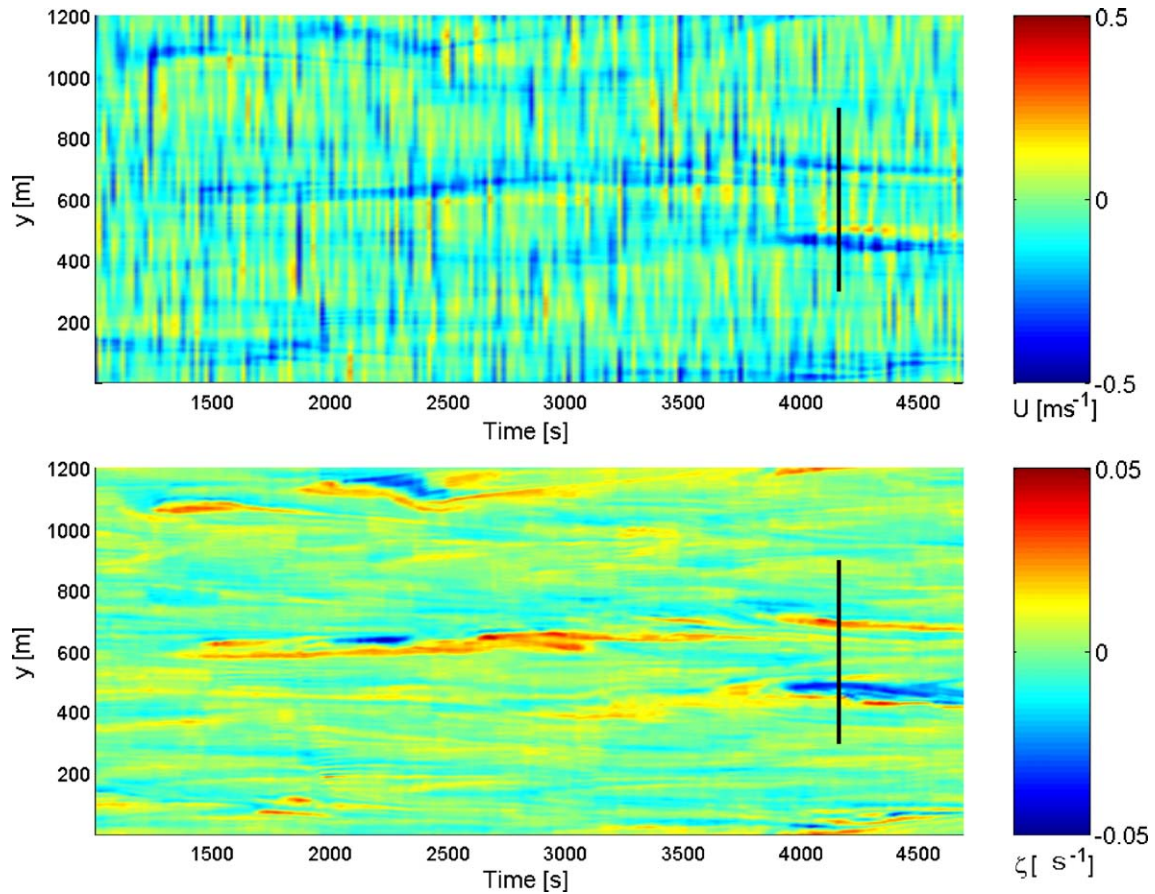


Fig. 8. Time-series of the cross-shore velocity and vorticity along the 2.0 m isobath for run 5 (0.03N10). The solid lines correspond to the snapshot of Fig. 5.

requires a careful definition of what constitutes a transient rip as distinct from other flow features. The key features of a rip current are defined to be:

- (1) Offshore flow of at least 0.15 ms^{-1} across the outer edge of the surfzone. This corresponds locally to an offshore mass flux that is approximately three times the wave-induced onshore flux.
- (2) Constrained offshore flow and associated opposite signed regions of high vorticity.
- (3) A period of continuous offshore flow exceeding 120 s.

Criterion 3 distinguishes a rip from a passing vortex couple which might exist without the jet region of a rip current. The rips are identified from the (y, t) plots (e.g. Fig. 8). To ensure objective consistency between different conditions, an algorithm was used to generate template of regions which satisfy criterion 1 and 2 in (y, t) space; the algorithm is described in the Appendix. To satisfy criterion 3, a rip is then defined as an unbroken template in (y, t) space with a duration of at least 120 s. From the series of templates, a number of statistics can then be generated:

- Duration — total length in time of the template.
- Mean current — mean offshore velocity over area covered by the template.

- Maximum current — maximum offshore velocity covered in the template.
- Maximum width — widest point of the template along the y direction.

The period of the simulation runs from 1000 to 4600 s is used to calculate statistics for the rips in runs 1 to 12. As the outer limit of breaking is around the 2.5 m isobath, this is set as an appropriate reference to investigate the rip current activity.

Fig. 11 shows the duration and mean offshore velocity of all the rip events passing the criteria across the 2.5 m isobath (the cross-shore horizontal distance to the 2.5 m isobath is of course dependent on the beach slope). There is significant variation of the number, duration and intensity of rip events between different spectra and beach slopes. There is an obvious increase in the duration and strength of rip currents for the long period narrow spread waves as the beach slope decreases. This corresponds well with the observations of Murray et al. (2003) (and personal communication) who found an increase of transient rip activity with decreasing beach slope for swell dominated conditions. By contrast, for the shorter period waves with wide spreading (W7 and W5), there is a decrease in rip frequency, strength and duration with decreasing beach slope. For the 0.015 slope there is a dramatic decrease in rip occurrence and strength from the swell dominated conditions

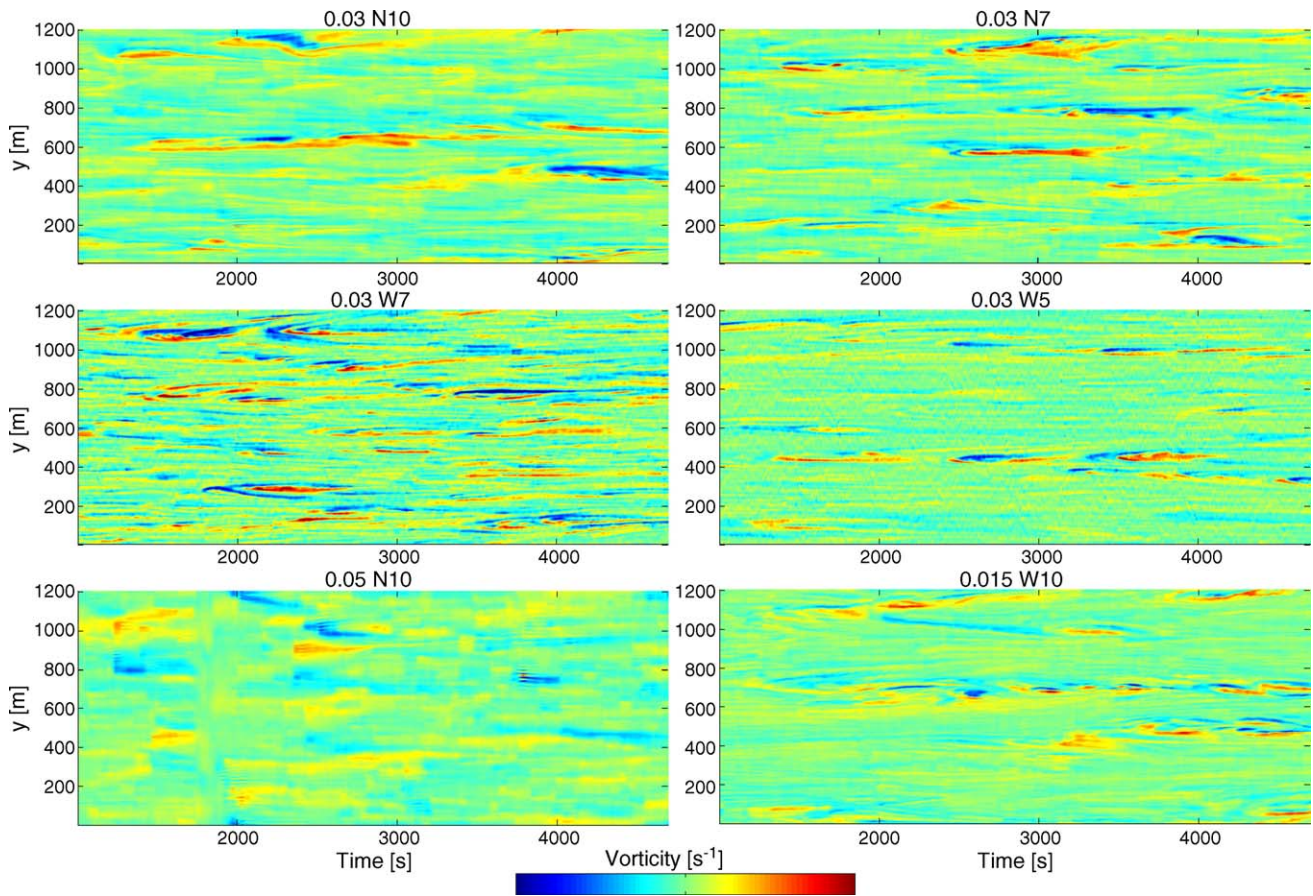


Fig. 9. Longshore vorticity time series on 2 m isobath for run 5 (0.03N10), 6 (0.03N7), 7 (0.03W7), 8 (0.03W5), 1 (0.05N10) and 9 (0.015N10).

to shorter period wave fields. Again this agrees in general terms with Murray et al. (2003), who found that for a beach with slope of 0.02, rip activity decreases as the standard deviation of wave height increases (in other words as the sea state becomes “messier”). There is no consistent effect of spreading for the same peak wave period, as differences between N7 and W7 vary with beach slope.

The mean and maximum velocity and widths of the transient rip population are shown in Fig. 12. The mean

value for the offshore velocity is surprisingly constant, but this may be partly related to the way in which a rip is defined and identified. The rip current widths show how short the typical longshore length scales are, and the mean appears to decrease for spectra with shorter peak period and increased spreading. While caution is required in relating specific values to field measurements, as they are somewhat determined by the rip selection process itself, the velocities and rip widths for 0.03N10 are consistent with field

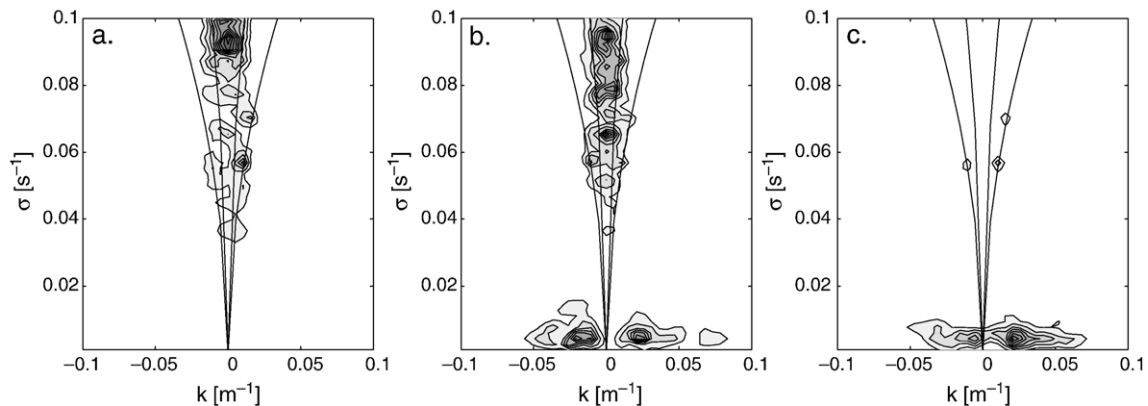


Fig. 10. Wave number-frequency spectra on the 2.0 m isobath for run 5(0.03N10). a. \bar{u} (contours $10^4 \text{ m}^3\text{s}^{-1}$) b. \tilde{U} (contours $10^4 \text{ m}^3\text{s}^{-1}$) c. V (contours $10^4 \text{ m}^3\text{s}^{-1}$). The lines are the dispersion relations for the first two edge wave modes.

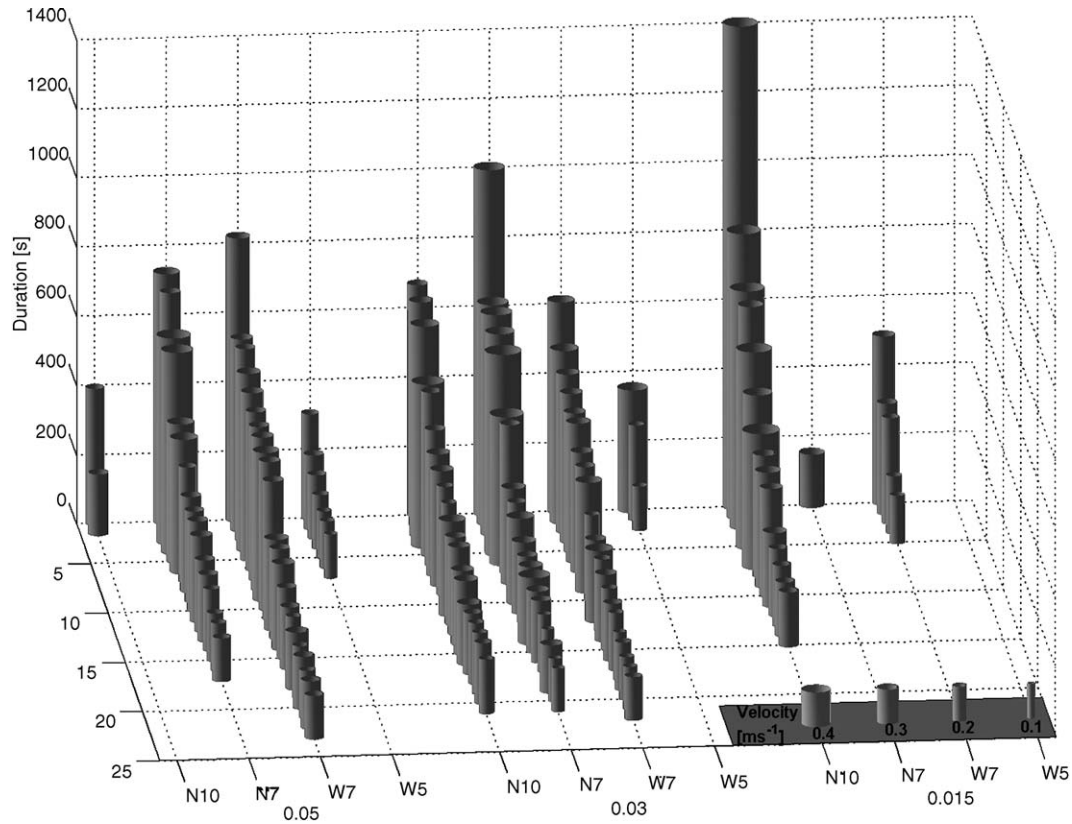


Fig. 11. Rip currents crossing the 2.5 m isobath for runs 1 to 12. Each column represents one continuous rip current, showing mean velocity and duration as indicated by width and height.

estimates (JP04) of the long-shore length scales of transient rip current neck regions.

6. Transient rip generation

The generation of an individual rip is shown in Fig. 13. The main sequence of features is common to all rip events seen in the data:

- (1) Two patches of vorticity within the surfzone with opposite rotations such that the patch in the positive y direction has a negative (clockwise) rotation.
- (2) Intensification of vorticity in each patch leading to a well defined vortex pair.
- (3) Propagation of the vortex pair offshore.
- (4) Further intensification of the vortex pair and movement of the vortices towards each other.
- (5) The formation of a rip neck behind the head region containing the vortex pair.
- (6) Shedding and dissipation of one or both vortices as the rip decays.

In the example shown in Fig. 13, a secondary vortex pair appears to be formed from the edges of the rip neck and maintains the rip as the first pair breaks off. The distance of penetration of the rip current beyond the surfzone is limited to just beyond the 3 m contour.

The fundamental behaviour of idealised patches of vorticity in a wedge shaped domain is relatively well understood and has been discussed by Peregrine (1998) and Bühler and Jacobson (2001) in reference to the surfzone. Individual vortices will tend to propagate longshore and the propagation direction means that the two patches seen in the initial stages of rip generation will tend to be driven together. A vortex pair rotating as seen here will also tend to propagate offshore into deeper water. As the vortex pair moves offshore, conservation of potential vorticity also means that streamlines will be squeezed together; this was proposed as the reason for offshore intensification of rip neck flow by Arthur (1962). The formation and shedding of vortex pairs from the edges of rip channels is also seen in simulations of topographic rip currents (e.g. Chen et al., 1999; Haas et al., 2003). Generation of vortex pairs occurs at the edges of the rip channel and they are subsequently advected offshore so that the rip periodically sheds vortex pairs into the region offshore of the bar. The fundamental dynamics of the vortex pairs, once initiated, appear to be qualitatively similar.

6.1. Vorticity balance

The dynamics of the vorticity are governed by the curl of Eq. (2),

$$\frac{\partial \bar{\zeta}}{\partial t} + (\bar{\mathbf{U}} \cdot \nabla) \bar{\zeta} = \bar{\zeta} \bar{\mathbf{U}} \cdot \frac{\nabla(\bar{\eta} + h)}{\bar{\eta} + h} + \nabla \times (\bar{\mathbf{S}} + \bar{\mathbf{L}} + \bar{\mathbf{B}}) \quad (26)$$

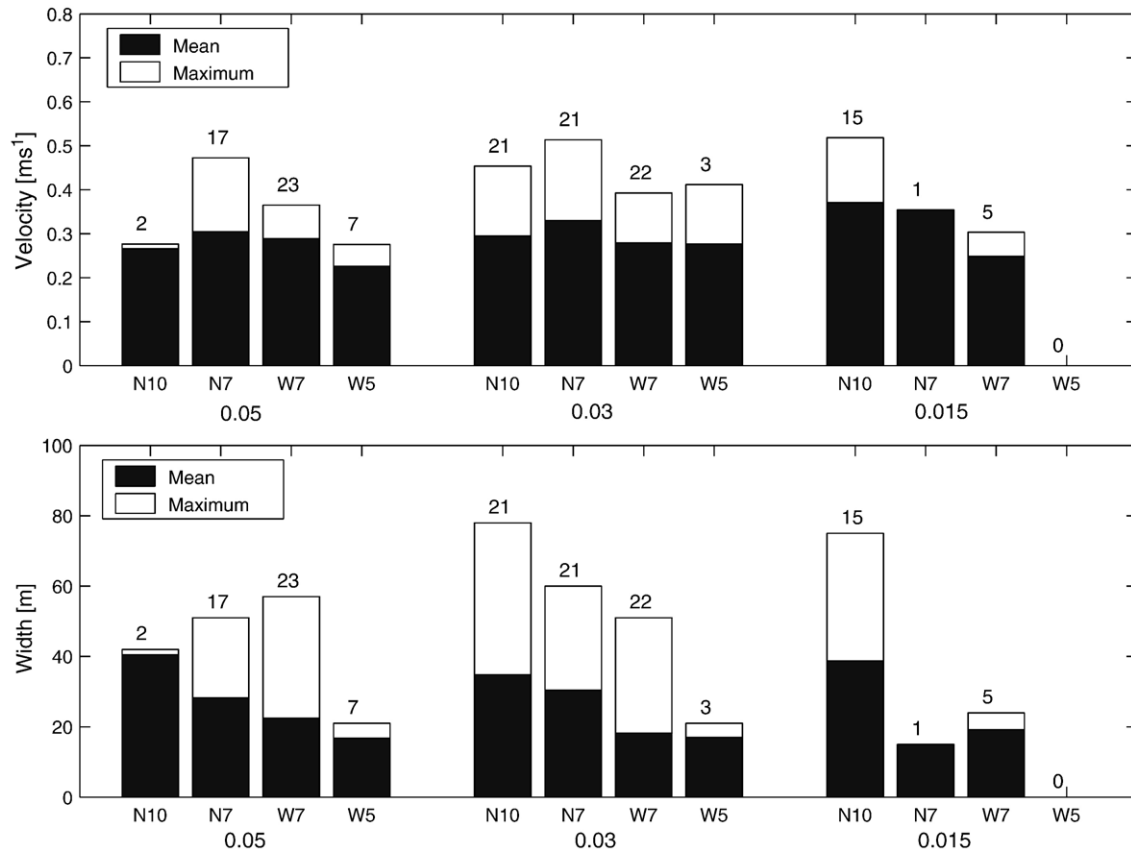


Fig. 12. Mean and maximum offshore velocity (top) and longshore width (bottom) of rip currents crossing the 2.5 m isobath for runs 1 to 12. The number of individual rip currents in each case are indicated at the top of each bar.

which can also be written as an equation for the potential vorticity:

$$\frac{D}{Dt} \left(\frac{\bar{\zeta}}{\bar{\eta} + h} \right) = \frac{1}{\bar{\eta} + h} \nabla \times (\bar{\mathbf{S}} + \bar{\mathbf{L}} + \bar{\mathbf{B}}) \quad (27)$$

Eq. (27) shows that new vorticity is provided to the current field through the $\nabla \times \mathbf{S}$ term as $\nabla \times \mathbf{L}$ and $\nabla \times \mathbf{B}$ are both dissipative. The lack of vorticity in run 17 strongly suggests that the directional spreading of the wave field is necessary to input the ambient vorticity necessary to generate coherent rotational features. Furthermore, the similarity of the rip positions for the same wave field (identical at the source line) but different beach slopes (0.03 and 0.015) seen in Fig. 9 suggests that incident wave/edge wave interaction is not a dominant factor in determining rip position as different slopes would have different edge wave mixes. Therefore, the inherent spatial variability (and hence breaking) of a random directionally spread wave field appears to be the dominant determination of $\nabla \times \mathbf{S}$ and hence where rip currents form. It is clear that the shedding of vorticity from breaking wave crests (Fig. 4) supplies new vorticity to the current field. This is the mechanism proposed by Peregrine (1998, 1999) in which a discontinuous bore generates vorticity at its end.

In the time series of vorticity evolution, snapshots of which are shown in Fig. 13, patches of existing vorticity can be seen to move around and coalesce within the surfzone. In addition,

there is advection of vorticity from the shore-line boundary deeper into the surfzone. The advective change of local vorticity is represented by the term $(\bar{\mathbf{U}} \cdot \nabla) \bar{\zeta}$ in Eq. (26).

It is useful to estimate the relative magnitude of terms in Eq. (26). All of the terms except $\nabla \times \mathbf{S}$ can be easily evaluated directly from the model results. The term $\nabla \times \mathbf{S}$ can in principle be calculated directly, however this is quite complex and it is easier to simply assume it is the residual in the local rate of change of vorticity once the other terms have been accounted for. Fig. 14 shows the relative magnitude of the nonlinear, stretching and forcing terms for varying cross-shore locations for the period ($t=3740-4540$ s) and longshore extent ($y=360-600$ m) of Fig. 13. The incident wave forcing term is the largest in the inner surfzone and decreases offshore, indicating that the main vorticity input from the incident wave field occurs in the inner surfzone. The nonlinear terms are also important in the inner surf zone but become increasingly dominant moving offshore. The stretching term is smaller and reduces offshore, corresponding to the decrease in $\nabla h/h$; however this term is important as it intensifies seaward moving vorticity.

The bottom friction term, $\nabla \times \mathbf{B}$, acts to dissipate vorticity and the lateral mixing term, $\nabla \times \mathbf{L}$, will tend to smear out vorticity gradients and discourage the formation of coherent features such as vortices. These terms are an order of magnitude smaller than the others, but act to spin down the transient rip flow.

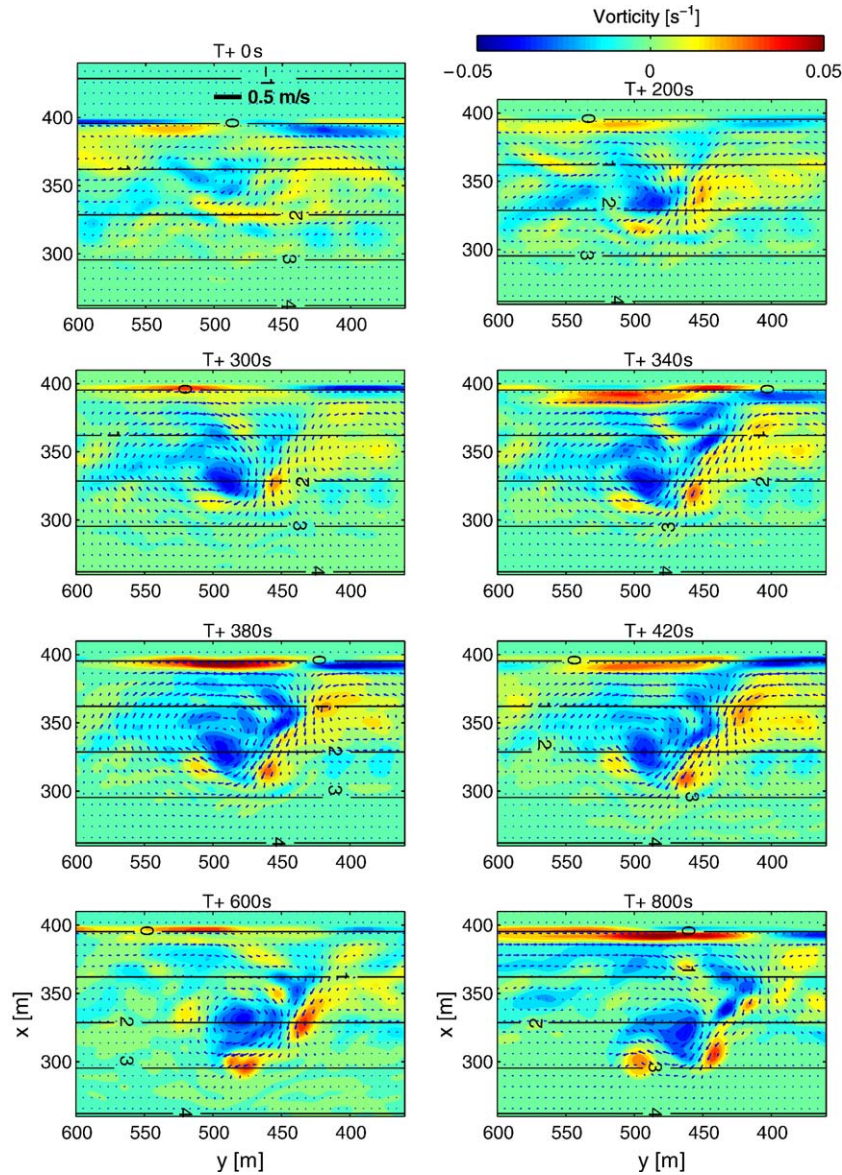


Fig. 13. Snapshots of the velocity and vorticity field for a section of run 5 (0.03N10) from time $t=3740$ s showing the development of a transient rip current.

6.2. Feedback

Rips are often seen to re-emerge from the same place as a previous rip. The persistence of the long narrow regions (in y, t space) of high vorticity associated with the rip currents are seen in Fig. 8. This is appears to be because remnant patches of vorticity encourage the spin-up of new vortex patches in the same location, as seen in the sequence in Figs. 13 and 14.

In (y, t) plots of the RMS surface elevation, σ_η , within in the surfzone (Fig. 15), although small in comparison the random variability, there is a clearly discernable signature of the rip currents, indicating that there is some feedback on the incident wave field. The RMS elevation is defined as $\sigma_\eta = \sqrt{(\eta - \bar{\eta})^2}$, so does not include slower variations of the wave-averaged elevation (such as infragravity waves).

Individual wave crests in the model appear to be refracted towards the centre of the rip current and there is local increase of crest height within the rip neck, similar to the observations of Chen et al. (1999) for monochromatic waves propagating over a topographic rip. This is consistent with the wave-averaged model results of Yu and Slinn (2003) and laboratory measurements of Haller et al. (2002) in topographic rip currents. As a result, there is negative feedback in the rip neck, but as the refracted waves break further offshore, positive feedback in the inner surfzone; the net effect is to encourage the formation of rips but then to limit their offshore penetration.

The lack of rip currents in run 17 suggests that for the frictional and mixing parameters used for the simulations, the feedback mechanism by itself is not unstable. An analysis by Falqués et al. (1999) found the setup in the wave-averaged

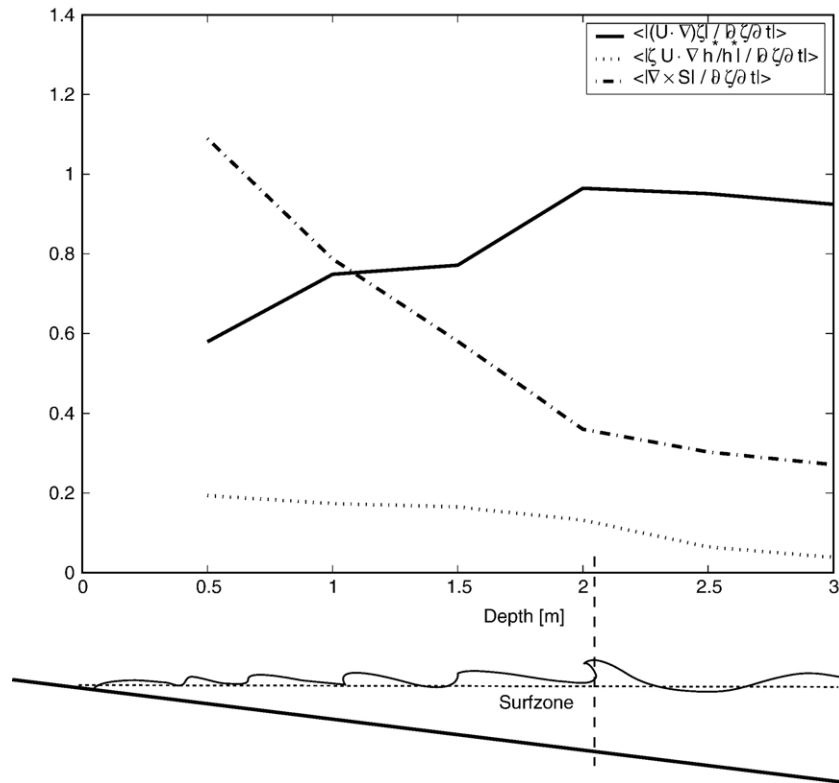


Fig. 14. Magnitude of terms in vorticity balance relative to the local rate of change of vorticity. The ratios of the absolute values of terms are calculated and then averaged over the temporal and longshore extent in Fig. 13 for cross-shore locations corresponding to the depth shown.

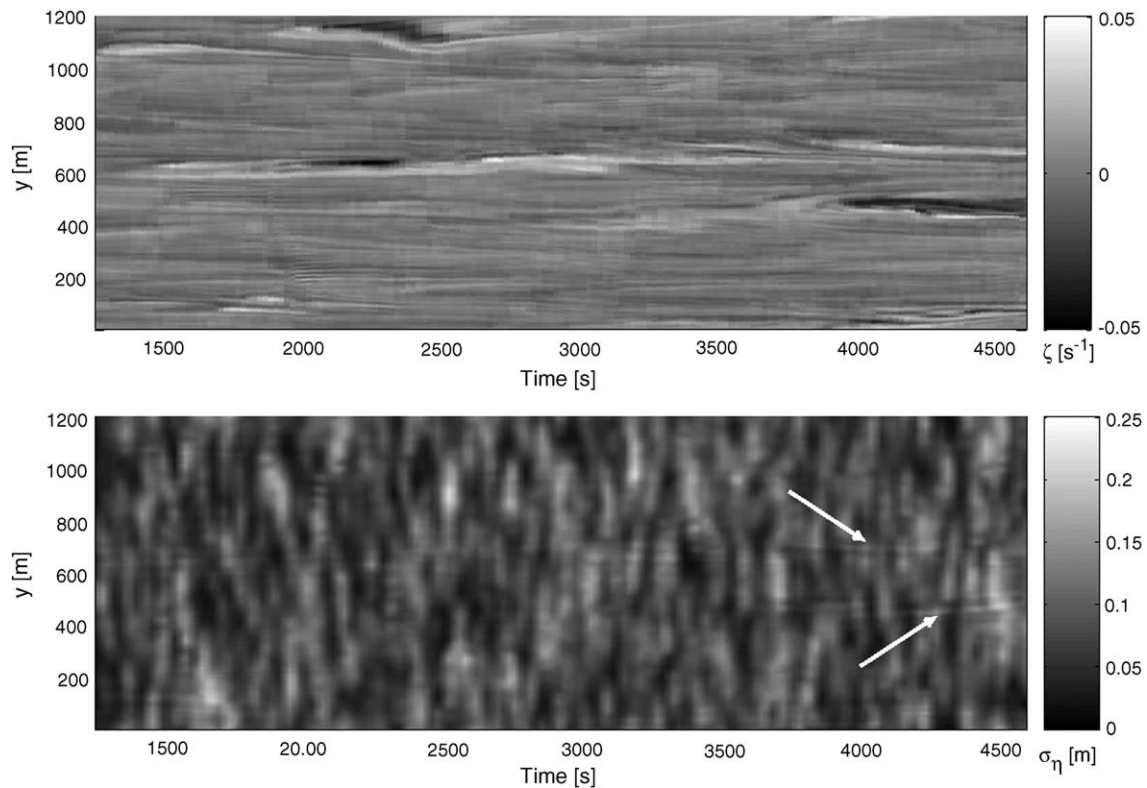


Fig. 15. Vorticity and RMS elevation (relative to wave-averaged elevation) on 2 m isobath for run 5 (0.03N10). The arrows highlight the influence of the vorticity on the incident wave heights elevations.

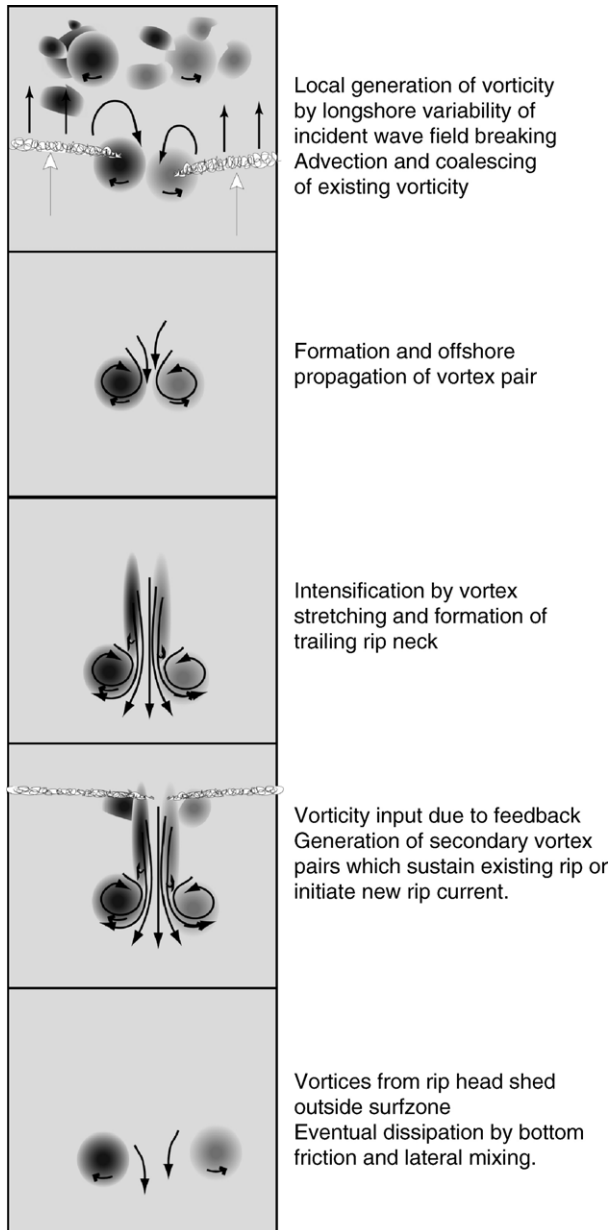


Fig. 16. Conceptual model of transient rip generation.

equations to be unstable to a idealised shore perpendicular wave field if there is feedback due to refraction of the incoming wave field. However, the results of run 17, effectively a slightly perturbed plane wave field with a spread of frequencies, show the opposite (refraction is implicitly included in the Boussinesq equations). The results here indicate that a certain amount of directional spreading, and the associated spatial gradients in forcing of the wave-averaged current, is required to provide sufficient vorticity to initiate the rip generation process. An interesting extension of the present work would be to test a full range of directional spreading at smaller increments, to find more exactly the minimum spreading required to initiate transient rips, and to get a more complete picture of how intensity and frequency of transient rips varies as the directional spreading varies.

To summarise the rip generation mechanism, a proposed conceptual model is shown in Fig. 16. The key feature is the formation of a vortex pair which propagates offshore. The generation of the regions of opposite signed vorticity is due both to direct input of vorticity from the incident wave field and advection of existing vorticity. A positive feedback means that new vorticity tends to be injected in the inner surfzone so as to enhance the existing vorticity distribution; this appears to lead to persistence and repeated development of rip currents at the same location.

7. Effect of bottom friction and subgrid mixing

A detailed investigation of the effect of the bottom friction and lateral mixing was not carried out. However for completeness, the bottom friction and lateral mixing parameters were varied by an order of magnitude in runs 13–16 to qualitatively understand how important these variations might be on the wave-averaged flow. The flow fields for run 5 and 13–16 after 10,000 time-steps is shown in Fig. 17. These runs are all with the same slope of 0.03 and spectra (peak period of 10 s and a spreading parameter of 100) to show the effect of varying the bottom friction coefficient and subgrid mixing coefficient.

The effect of increasing both parameters is to reduce both the magnitudes and gradients of the discrete rotational flow features. An order of magnitude increase of the bottom friction coefficient appears to be more significant than an equivalent increase of mixing coefficient, as seen in Fig. 17 subplots *b* and *d*. The effect of reduced bottom friction (subplot *c*) is interesting as it appears to somewhat alter the flow pattern and vorticity patches are less well defined. Decreasing the subgrid mixing parameter appears to have the least effect of all the variations, with the same flow pattern seen (subplot *e*).

It is important to note that the lateral mixing caused by the shear dispersion mechanism of Svendsen and Putrevu (1994) is not included in the Boussinesq model. Sensitivity of modelled rip currents to bottom friction and lateral mixing (including shear dispersion mixing effect) was tested by Haas et al. (2003). These comparisons were for wave-averaged model simulations of tank scale rip currents and found that both increased bottom friction and lateral mixing tend to stabilise the rip currents and decrease peak current speeds. In numerical wave-averaged experiments of rip currents formed over an idealised bar/trough topography, Yu and Slinn (2003) found bottom friction less important and that wave-current interaction was dominant in determining the flow patterns.

The differences in flow patterns, albeit for order of magnitude differences in values, highlight the importance of using the correct parameters for any accurate simulations of real situations. The results generated with the parameters used for the main simulations may not be entirely accurate for the precise prediction of velocities. However, the fact that the general shape and features of the flow field remains unaltered suggests that fundamental mechanisms discussed in Section 6 are unaltered by varying parameters. Furthermore, it seems reasonable to assume that the quantitative comparison in Section 5 should remain valid in a *relative* sense.

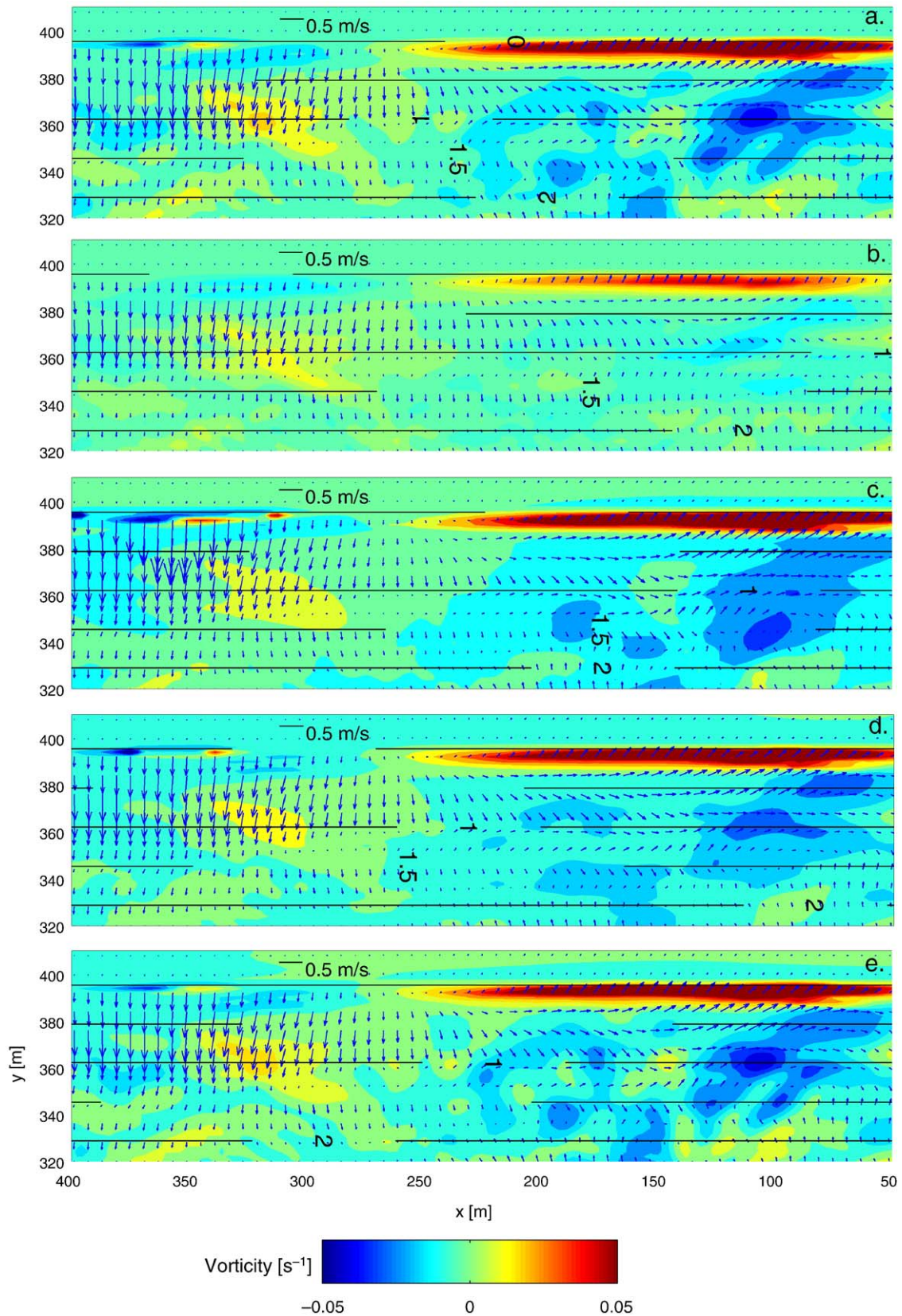


Fig. 17. Velocity field from runs 5, 13–16 (top to bottom) 1000 s after the start of the simulation for the spectra N10 and beach slope 0.03 but with varying friction and mixing parameters (f_b and c_m). From the top to bottom the friction and turbulent mixing parameters are a. $f_b=0.001$, $c_m=0.2$, b. $f_b=0.01$, $c_m=0.2$, c. $f_b=0.0001$, $c_m=0.2$, d. $f_b=0.001$, $c_m=2.0$, e. $f_b=0.001$, $c_m=0.02$.

8. Infragravity turbulence

An interesting observation which arises from the results is of spatially and temporally variable currents that, while containing well-defined features such as transient rips, appear quite random. Peregrine (1998) has suggested that flow in the nearshore may have the character of two dimensional turbulence. The rotational flow component of the wave-averaged nearshore currents may have similarities with forced quasi two-dimensional turbulence (“quasi” as the flow is not truly two-dimensional) in a wedge shaped domain.

The magnitude of the terms in the vorticity equation (which have similar relative magnitudes if the analysis in Section 6.1 is extended to the whole domain) suggest that nonlinear transfer of vorticity is of similar importance to the incident wave forcing. The rotational flow response would then be the combined effect of a (linear) response to the forcing at a range of scales and readjustment of energy between scales by nonlinear turbulent type mechanisms. Identification of nonlinear energy transfer between scales, which is the key characteristic of turbulence, is made difficult by the presence of a whole range of forcing scales in the incident wave field, but would be an important subject of future work.

If turbulent type mechanisms are important, the transient rips may be a coherent jet structure that naturally arises in variably forced two-dimensional turbulence (Danilov and Gurarie, 2001). It is possible that the incident forcing need not have a particular form, and that just “stirring” at an appropriate range of length scales leads to spontaneous formation of jets that are ejected offshore. The tendency of two-dimensional turbulence to form larger vortices from smaller vortices may explain observations in the model results of the agglomeration of small vorticity patches into larger ones. This would also provide an explanation for the observation in the previous section of a reduced bottom friction appearing to give larger more uniform patches of vorticity, as advection velocities are slightly stronger.

Beyond the fundamental behaviour of the rotational component of the flow, there is also the question of interaction between the rotational and divergent (long-wave) current components. As shown by Kirby et al. (1998b), edge and shear wave modes can form resonant sets. The spectra in Fig. 10 suggest that in the absence of shear waves, the rotational and divergent components are well separated in wave number-frequency space, which may mean that they can be decoupled and treated separately. However, this needs further investigation.

9. Summary and conclusions

Boussinesq model simulations of directionally spread random waves with the mean direction perpendicular to a plane beach show the development of a rotational current field not associated with infragravity waves or shear waves. Coherent features observed in the rotational flow field include transient rip currents and discrete vortices, which

occur variably in space and time. The exact nature of the flow field is dependent on the beach slope and the incident wave spectra. The frequency, duration, and intensity of the transient rip currents similarly depend on both the beach slope and the incident wave spectra. Transient rip activity increases with shallower beach slopes, and is greatest in a swell type wave field with narrow directional spread and longer peak period.

The transient rip currents are associated with a vortex pair which is generated within the surf zone and subsequently propagates offshore. Analysis of the vorticity balance show that the main vorticity input occurs within the inner surfzone. The vorticity dynamics during the evolution of the transient rip currents are strongly influenced by the advection terms, which makes precise identification of vorticity input difficult; however, observations of vorticity associated with discontinuities in incident wave crests suggest that this mechanism is important. The directional spreading of the wave field is necessary to initiate the transient rip currents, although their development and maintenance appears to involve a feedback mechanism which encourages persistence and repeated ejection from nearby locations.

The importance of transient rips and large scale horizontal vortices for applied coastal engineering are their contribution to mixing and cross-shore flux of material across the surfzone. As shown by Reniers et al. (2004), these currents may play a key role in beach morphology and stability, in particular the development of topographic rip current systems. In large scale coastal process models, the effect of transient rotational flow is in addition to cross-shore fluxes due to undertow or fixed rip currents but entirely missing in a classical wave-averaged description; further work is desirable to develop suitable parameterisations. Better understanding of transient rips also has an important public safety implication, as rip currents are often responsible for drowning deaths. While not as strong as large topographic rip currents, transient rips are potentially more dangerous, as they cannot be marked with fixed warning signs on the beach. Further investigation of transient rips may enable the development of a simple ‘transient rip index’, based the sea state and beach slope, that could be used as a management tool by lifeguards in assessing beach safety.

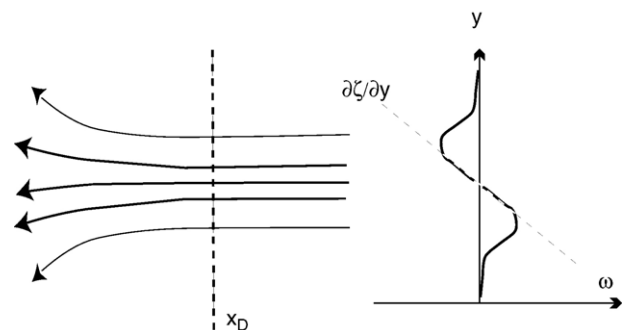


Fig. 18. Vorticity distribution across a rip current. In the coordinate system of the simulations, there is a negative gradient across the rip neck.

Acknowledgments

All of the modelling was carried out using a modified version of *Funwave 2D* from *Center for Applied Coastal Research, University of Delaware*. We gratefully acknowledge the high quality source code and documentation that is freely available to the scientific community. All of the simulations were carried out on a high performance computer at the Western Australian Interactive Virtual Environments Centre (IVEC). This work was carried out while D. Johnson was in receipt of a University Postgraduate Award (International) from the University of Western Australia. This is contribution ED1526 from the Centre for Water Research, University of Western Australia.

Appendix A

The rip identification algorithm is based on the principle that due to the regions of opposite signed vorticity, there is a strong vorticity gradient across the rip neck as shown in Fig. 18. For the closest offshore line of grid points for a given depth at location x_D , $\bar{U}(y_i, t_j; x_D)$ and $\bar{\zeta}(y_i, t_j; x_D)$ are vorticity and velocity values at longshore location y_i for each averaging period at time t_j (as plotted in Fig. 8). The procedure to identify the rips is:

- (1) For a minimum offshore velocity of U_T and a vorticity gradient threshold of $(\partial\bar{\zeta}/\partial y)_T$, mark $[y_i, t_j]$ bins where:

$$\bar{U}(y_i, t_j; x_D) \leq U_T \quad (28)$$

$$[\bar{\zeta}(y_i + 1, t_j; x_D) - \bar{\zeta}(y_i - 1, t_j; x_D)] / 2\Delta x \leq (\partial\bar{\zeta}/\partial y)_T \quad (29)$$

- (2) Define individual patches as a set of marked bins which are connected.
- (3) Discard all patches with total duration of less than 120 s.

The values of $U_T = -0.15 \text{ ms}^{-1}$ and $(\partial\bar{\zeta}/\partial y)_T = 0.0015$ are used. These values were found by tuning the performance of the algorithm so that well defined, jet-like vortical flows were found; this part of the procedure is subjective, however once the values are set, the process is consistent between the different runs.

References

- Allen, J., Newberger, P., Holman, R., 1996. Nonlinear shear instabilities of alongshore currents on plane beaches. *J. Fluid Mech.* 310, 181–213.
- Arthur, R., 1962. A note on the dynamics of rip currents. *J. Geophys. Res.* 67, 2777–2779.
- Bouws, E., Günther, H., Rosenthal, W., Vincent, C., 1985. Similarity of the wind wave spectrum in finite depth 1. Spectral form. *J. Geophys. Res.* 90 (C1), 975–986.
- Bowen, A., 1969. Rip currents 1. Theoretical investigations. *J. Geophys. Res.* 74 (23), 5479–5490.
- Bowen, A., Inman, D., 1969. Rip currents 2. Laboratory and field observations. *J. Geophys. Res.* 74 (C3), 5479–5490.
- Bühler, O., Jacobson, T., 2001. Wave-driven currents and vortex dynamics on barred beaches. *J. Fluid Mech.* 449, 313–339.
- Chen, Q., Dalrymple, R., Kirby, J., Kennedy, A., Haller, M., 1999. Boussinesq modelling of a rip current system. *J. Geophys. Res.* 104, 20617–20637.
- Chen, Q., Kirby, J., Dalrymple, R., Kennedy, A., Chawla, A., 2000. Boussinesq modeling of wave transformation, breaking and runup. II: 2d. *J. Wtrwy., Port, Coast. and Ocean Eng.*, vol. 126 (1), pp. 48–56.
- Chen, Q., Kirby, J., Dalrymple, R., Kennedy, A., Thornton, E., Shi, F., 2001. Boussinesq modelling of waves and longshore currents under field conditions. *Proc 27th Int. Conf. on Coast. Eng.*, pp. 651–663.
- Chen, Q., Kirby, J., Dalrymple, R., Shi, F., Thornton, E., 2003. Boussinesq modeling of longshore currents. *J. Geophys. Res.* 108 (C11), 3362, doi:10.1029/2002JC001308.
- Dalrymple, R., 1975. A mechanism for rip current generation on an open coast. *J. Geophys. Res.* 80, 3485–3487.
- Dalrymple, R., Lozano, C., 1978. Wave current interaction models for rip currents. *J. Geophys. Res.* 83 (C12), 6063.
- Danilov, S., Gurarie, D., 2001. Forced two-dimensional turbulence in spectral and physical space. *Phys. Rev., E Stat. Phys. Plasmas Fluids Relat. Interdiscip. Topics* 63, 061208.
- Falqués, A., Montoto, A., Vila, D., 1999. A note on hydrodynamic instabilities and horizontal circulation in the surfzone. *J. Geophys. Res.* 104 (C9), 20605–20615.
- Fowler, R., Dalrymple, R., 1991. Wave group forced nearshore circulation. *Proc 22nd Int. Conf. on Coast. Eng.*, vol. 1, pp. 729–742.
- Haas, K., Svendsen, I., Haller, M., Zhao, Q., 2003. Quasi-three-dimensional modeling of rip current systems. *J. Geophys. Res.* 108 (C7), 3217.
- Haller, M., Dalrymple, R., Svendsen, I., 2002. Experimental study of nearshore dynamics on a barred beach with rip channels. *J. Geophys. Res.* 107 (C6), doi:10.1029/2001JC000955.
- Hammack, J., Scheffner, N., Segur, H., 1991. A note on the generation and narrowness of periodic rip currents. *J. Geophys. Res.* 96 (C3), 4909–4914.
- Hughes, S., 1993. Physical models and laboratory techniques in coastal engineering. *Advanced Series on Ocean Engineering*, vol. 7. World Scientific, Singapore.
- Isobe, M., Kondo, K., Horikawa, K., 1984. Extension of MLM for estimating directional wave spectrum. Paper no. A-6. 15pp. *Proc. Symp. on Description and Modeling of Directional Seas*.
- Johnson, D., Pattiaratchi, C., 2004. Transient rip currents and nearshore circulation on a well dominated beach. *J. Geophys. Res.* 109 (C02026), doi:10.1029/2003JC001798.
- Kennedy, A.B., Kirby, J.T., 2003. An unsteady wave driver for narrow-banded waves: modeling nearshore circulation driven by wave groups. *Coast. Eng.* 48, 257275.
- Kennedy, A., Chen, Q., Kirby, J., Dalrymple, R., 2000. Boussinesq modeling of wave transformation, breaking and runup. i:1d. *J. Wtrwy., Port, Coast. and Ocean Eng.*, vol. 126 (1), pp. 39–47.
- Kirby, J., Chen, Q., 2003. Examining the low frequency predictions of a Boussinesq wave model. *Proc. 28th Int. Conf. On Coast. Eng.*, vol. 1. World Scientific, Singapore, pp. 1075–1087.
- Kirby, J., Wei, G., Chen, Q., Kennedy, A., Dalrymple, R., September 1998a. *Funwave 1.0; fully nonlinear Boussinesq wave model documentation and user's manual*. Tech. Rep. CACR-98-06, Center for Applied Coastal Research, University of Delaware, Newark, DE 19716.
- Kirby, J.T., Putrevu, U., Ozkan Haller, H.T., 1998b. Evolution equations for edge waves and shear waves on longshore uniform beaches. *Proc. 26th Int. Conf. On Coast. Eng.*, vol. 1. ASCE, pp. 203–216.
- LeBlond, P., Tang, C., 1974. On energy coupling between waves and rip currents. *J. Geophys. Res.* 79, 811–816.
- Madsen, P., Schaffer, H., 1998. Higher-order Boussinesq-type equations for surface gravity waves: derivation and analysis. *Philos. Trans. R. Soc. Lond.* A356, 3123–3184.
- Mitsuyasu, H., 1975. Observation of the directional wave spectrum of ocean waves using a cloverleaf buoy. *J. Phys. Oceanogr.* 5, 750–760.
- Murray, A., LeBars, M., Guillon, C., 2003. Tests of a new hypothesis for non-bathymetrically driven rip currents. *J. Coast. Res.* 19, 269–277.
- Oltman-Shay, J., Howd, P., 1989. Shear instabilities of the mean longshore current 2. Field observations. *J. Geophys. Res.* 94 (C12), 25–45.

- Ozkan-Haller, H., Kirby, J., 1999. Nonlinear evolution of shear instabilities of the longshore current: a comparison of observations and computations. *J. Geophys. Res.* 104 (C11), 25953–25984.
- Peregrine, D., 1998. Surf zone currents. *Theoret. Comput. Fluid Dyn. J.* 10, 295–309.
- Peregrine, D., 1999. Large-scale vorticity generation by breakers in shallow and deep water. *Eur. J. Mech. B, Fluids* 18, 403–408.
- Reniers, A., Roelvink, J., Thornton, E., 2004. Morphodynamic modeling of an embayed beach under wave group forcing. *J. Geophys. Res.* 109 (C01030), doi:10.1029/2002JC001586.
- Sasaki, T., Horikawa, K., 1978. Observation of nearshore current and edge waves. *Proc. 16th Int. Conf. On Coast. Eng. ASCE*, pp. 791–809.
- Shi, F., Kirby, J., Dalrymple, R., Chen, Q., 2003. Wave simulations in Ponce de Leon inlet using Boussinesq model. *J. Wtrwy, Port, Coast. and Ocean Eng.*, vol. 129 (3), pp. 124–135.
- Smagorinsky, J., 1963. General circulation experiments with the primitive equations. *Mon. Weather Rev.* 93, 99–165.
- Svendsen, I., Putrevu, U., 1994. Nearshore mixing and dispersion. *Proc. R. Soc. Lond. A* 545, 561–576.
- Symonds, G., Ranasinghe, R., 2001. On the formation of rip currents on a plane beach. *Proc. 27th Int. Conf. On Coast. Eng.*, vol. 1. ASCE, pp. 468–481.
- Tang, E.-S., Dalrymple, R., 1989. Nearshore circulation: rip currents and wave groups. *Advances in Coastal and Ocean Engineering*. Plenum Press, New York, pp. 205–230.
- van Dongeren, A., Reniers, A., Battjes, J., Svendsen, I., 2003. Numerical modeling of infragravity wave response during Delilah. *J. Geophys. Res.* 108 (C9), doi:10.1029/2002JC001332.
- Wei, G., Kirby, J., Grilli, S.T., Nd Subraymanya, R., 1995. A fully non-linear Boussinesq model for surface waves: I. Highly non-linear, unsteady waves. *J. Fluid Mech.* 294, 71–92.
- Wei, G., Kirby, J., Sinha, A., 1999. Generation of waves in Boussinesq models using a source function method. *Coast. Eng.* 36, 271–299.
- Yu, J., Slinn, D., 2003. Effects of wave-current interaction on rip currents. *J. Geophys. Res.* 108 (C3), 3088, doi:10.1029/2001JC001105.